

VILJAR PALMRE

Fabrication and characterization
of microporous carbon-based electroactive
polymer actuators



TARTU UNIVERSITY PRESS

Institute of Chemistry and Institute of Technology, University of Tartu, Estonia

The dissertation was admitted on June 19, 2012 in partial fulfillment of the requirements for the degree of Doctor of Philosophy in Material Science, and allowed for defense by the Scientific Council on Material Science of the Faculty of Science and Technology of the University of Tartu.

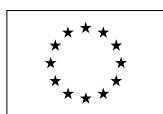
Supervisors: Prof. Enn Lust, Institute of Chemistry,
University of Tartu, Estonia

Prof. Alvo Aabloo, Institute of Technology,
University of Tartu, Estonia

Opponent: Prof. Ari Ivaska, Åbo Akademi University, Finland

Commencement: August 21, 2012 at University of Tartu, Tartu, Estonia

This work has been partially supported by Graduate School „Functional materials and technologies“ receiving funding from the European Social Fund under project 1.2.0401.09–0079 in University of Tartu, Estonia.



European Union
European Social Fund



Investing in your future

ISSN 2228–0928

ISBN 978–9949–32–057–8 (trükis)

ISBN 978–9949–32–058–5 (PDF)

Autoriõigus: Viljar Palmre, 2012

Tartu Ülikooli Kirjastus

www.tyk.ee

Tellimus nr. 356

CONTENTS

LIST OF ORIGINAL PUBLICATIONS	6
1. INTRODUCTION	7
2. STATE OF THE ART	9
2.1. Brief overview of electroactive polymers (EAPs)	9
2.2. Potential applications of EAPs	10
2.3. Ionic EAPs	11
2.3.1. Fabrication methods	11
2.3.2. Electrode materials	15
3. EXPERIMENTAL	18
3.1. Fabrication of EAP actuators by Direct Assembly Process	18
3.1.1. Materials and chemicals used	18
3.1.2. Preparation of actuator elements	19
3.2. Fabrication of EAP acutators by Layer-by-layer casting technique .	21
3.2.1. Materials and chemicals used	21
3.2.2. Preparation of actuator elements	22
3.3. Characterization	23
3.3.1. EAPs prepared by Direct Assembly Process	23
3.3.2. EAPs prepared by layer-by-layer casting technique	25
4. RESULTS AND DISCUSSION	27
4.1. Comparison of different electrode material properties	27
4.2. Effects of carbon nanotube additives in carbide-derived carbon electrodes	35
5. SUMMARY	43
6. REFERENCES	45
7. SUMMARY IN ESTONIAN	49
8. ACKNOWLEDGEMENTS	51
9. ORIGINAL PUBLICATIONS	53

LIST OF ORIGINAL PUBLICATIONS

This Dissertation is a summary based on the following original publications, which are referred to by Roman numerals in the text:

- I. **V. Palmre**, D. Brandell, U. Mäeorg, J. Torop, O. Volobujeva, A. Punning, U. Johanson, M. Kruusmaa, A. Aabloo, Nanoporous carbon-based electrodes for high strain ionomeric bending actuators. *Journal of Smart Materials and Structures* 18 (2009) 095028.
- II. **V. Palmre**, E. Lust, A. Jänes, Mihkel Koel, A.-L. Peikolainen, J. Torop, U. Johanson, A. Aabloo, Electroactive polymer actuators with carbon aerogel electrodes. *Journal of Materials Chemistry* 21 (2011) 2577–2583.
- III. **V. Palmre**, U. Johanson, M. Kruusmaa, A. Aabloo, Actuator and method of its fabrication. Estonian Patent Application, EE200800011. Patent pending in Estonia, patent application published 15.10.2009.
- IV. **V. Palmre**, J. Torop, M. Arulepp, T. Sugino, K. Asaka, A. Jänes, E. Lust, A. Aabloo, Impact of carbon nanotube additives on carbide-derived carbon-based electroactive polymer actuators. *Carbon* (2012). In Press.

Author's contribution

Paper I and II: The author fabricated all the EAP actuator samples used in the studies, performed their electromechanical, -chemical and mechanical characterizations, processed and interpreted the data, and wrote the papers.

Paper III: The author fabricated EAP actuator samples and performed their electromechanical, -chemical and mechanical characterizations, contributed to writing.

Paper IV: The author processed and interpreted the data, and wrote the paper.

Other publications

- V. J. Torop, M. Arulepp, J. Leis, A. Punning, U. Johanson, **V. Palmre**, A. Aabloo, Nanoporous carbide-derived carbon material-based linear actuators. *Materials* 3 (1) (2010) 9–25.
- VI. J. Torop, **V. Palmre**, M. Arulepp, T. Sugino, K. Asaka, A. Aabloo, Flexible supercapacitor-like actuator with carbide-derived carbon electrodes. *Carbon* 49 (9) (2011) 3113–3119.
- VII. A. Aabloo, F. Kaasik, **V. Palmre**, J. Torop, Layered actuator. WO 2011/050820 A2.

I. INTRODUCTION

Electroactive polymers (EAPs) are a type of smart materials that convert electrical pulse energy into mechanical deformation or *vice versa*, and hence, can be utilized as actuators or sensors.

EAPs are promising functional materials for engineering new and increasingly demanded actuation systems that are silent, mechanically compliant, lightweight, structurally simple, and easily scalable. Conventional actuators such as electromagnetic and pneumatic/hydraulic drives cannot offer these features due to considerably different operating principles involved and fabrication paradigms associated with down-scaling. EAPs with their simplicity can be manufactured in various shapes and sizes down to microscale. There are many technological fields that can benefit from the unique properties of EAP materials. EAP actuators and sensors have been explored particularly for applications in medicine, space technology, and robotics [1–3]. Since they mimic the behavior of biological muscles, EAP actuators are attractive for creating artificial muscles for biologically inspired robots, especially for underwater applications [3, 4].

EAPs are generally divided in two principal classes: dielectric and ionic. In this dissertation, we studied ionic type of EAP actuators, in which the actuation is generated by electric field induced displacement of ions.

One of the prevailing ionic EAPs are ionic polymer-metal composites (IPMCs) that have received considerable attention during the last two decades, primarily due to their inherent large bending deformation and low driving voltage (1–4 V) [2, 5–8]. IPMC consists of thin ionic polymer membrane covered on both surfaces with noble metal (Pt or Au) electrodes. However, a wider deployment of these materials is limited mainly because of their complex manufacturing and unstable operation that results from the evaporation and electrolysis of inner solvent (mainly water). Therefore, a lot of effort has been focused on developing manufacturing techniques that allow using less expensive electrode materials and more stable solvents and electrolytes such as ionic liquids. Recently Fukushima and Asaka *et al.* [9] came up with so-called layer-by-layer casting technique for fabrication of ionic liquid containing actuators with single-walled carbon nanotube (SWCNT) electrodes. Later, Akle *et al.* [10] introduced a new manufacturing technique, called Direct Assembly Process (DAP), in which the porous RuO_2 electrodes were directly painted onto ionic liquid-impregnated Nafion membrane and hot-pressed. Both of these methods offer simplicity and control over the process, and flexibility to use various electrode materials for assembling EAP actuators.

It is commonly accepted that the increase of charge density within the electrodes leads to higher actuation performance of an EAP actuator. In this work, significant efforts have been put into exploring highly porous conductive materials for assembling EAP actuators with high specific surface area electrodes. The materials with highest potential for this purpose are highly

porous amorphous carbons and carbide-derived carbons (CDC), commonly used in energy storage devices – supercapacitors. CDC is produced by extraction of metal ions from metal carbides via chlorination at elevated temperature, and has well-defined microporous structure, very high specific surface area, and excellent electrochemical stability [11–14].

In this thesis, coconut shell-based activated carbon and carbide-derived carbon were studied for application as electrode materials in EAP actuator systems. In addition, less expensive alternative materials – activated and non-activated carbon aerogels – were investigated for creating high specific surface area electrodes for the actuators. Carbon aerogel is a highly porous material obtained by the pyrolysis of organic aerogel [15]. Further, the actuator elements based on RuO₂ electrodes, first introduced by Akle *et al.* [10], were also prepared in-house and used as reference systems for comparison. All the actuator elements were fabricated using the direct assembly process, and were composed of ionic liquid-impregnated Nafion membrane between the two porous electrode layers and gold foil on the surface. The electromechanical, -chemical and mechanical characteristics of the prepared EAPs were measured and comparatively analyzed.

The second part of this dissertation is focused on studying the effects of SWCNT additives in CDC electrodes of the EAP actuator. The SWCNTs were used as an additive to increase the mesoporosity and electronic conductivity of the CDC electrodes. This is to enhance the electrolyte diffusion into micropores and accessibility of the surface that in turn should lead to increased charging rates and thereby improves the actuation response of the EAPs. To examine the effects of SWCNTs on the actuation performance, the EAPs with various ratios of SWCNTs to CDC in the electrodes were fabricated, while keeping the total wt.% of carbon material constant. The actuator elements were prepared by Layer-by-layer casting technique and were composed of polymer/ionic-liquid membrane between two conductive SWCNT/CDC electrode layers. The electromechanical and electrochemical properties of the prepared SWCNT/CDC-actuators with different electrode compositions were discussed and analyzed.

2. STATE OF THE ART

2.1. Brief overview of electroactive polymers (EAPs)

Several types of polymeric materials can convert electrical energy into mechanical energy. The examples of such materials include piezoelectric polymers, dielectric elastomers, shape memory polymers, conducting polymers, bucky gels, ionic polymers, and polymer gels. All the mentioned EAP materials have their own advantages and disadvantages and are each suited for different applications.

Piezoelectric polymers are semicrystalline materials that can maintain permanent electric polarization [16]. Polyvinylidene fluoride (PVDF) and its copolymers are one of the best known piezoelectric polymers exhibiting highest strain response at room temperature. The actuation in piezoelectric polymers is initiated by orientation of asymmetric crystals (dipoles) in response to applied electric field. Piezoelectric actuators operate at high frequencies and generate relatively high stress. The main disadvantages are small strain response (micron scale) and high operating voltage (in the range of 1 kV). Therefore, these materials are mainly suited for applications requiring small displacements such as positioning objects with high precision.

Dielectric elastomers represent a large category of EAPs [17], and are composed of elastomer film sandwiched between two compliant conductive electrodes. Application of electric field (100 MV/m) generates electrostatic pressure due to Coulomb forces between the electrodes that squeezes the elastomer film. Dielectric elastomers can generate very high strains ($> 100\%$) and high stresses depending on the elasticity of elastomer, and are simple to fabricate. For the acrylic elastomer VHB 4910TM, a strain more than 300% has been observed [18]. The main disadvantages of dielectric elastomers are high operating voltage and low reliability.

Shape memory polymers (SMPs) can memorize temporary shape(s) and recover their original (permanent) shape when exposed to temperature change [19]. The reversible phase (shape) transitions are induced by heating and cooling the material. Shape memory polymers can be actuated electrically via resistive heating, and exhibit large strain ($> 100\%$) and moderate stress. However, SMPs have slow strain response, require high operating temperatures and are limited by the number of shapes it can memorize. The materials that exhibit shape memory effect include thermosets and thermoplastics.

Intrinsically conducting (or conjugated) polymers (ICPs) are another large category of EAPs [20–22]. Conducting polymers are electronically conductive organic materials with conjugated structures. One of the extensively studied ICPs are polypyrrole (PPy), polythiophene (PTh), polyaniline (PANi) and their copolymers. The actuation of ICPs is based on reversible redox reactions. Applied electric potential leads to addition or removal of charge from the polymer backbone and causes transport of electrolyte ions to balance the charge. The displacement of ions is accompanied by volume change that generates

actuation. Conductive polymers are attractive EAP materials as they produce relatively large strains and low or moderate stresses under low applied voltage (~ 2 V). The main disadvantages are slow actuation response and low cycle life.

Ionic polymers plated with two metal electrodes are commonly referred to as ionic polymer-metal composites (IPMCs) [2, 6], as introduced earlier. Actuation of this type of actuators is caused by swelling of the ionic polymer membrane on the cathode side and shrinkage of that on the anode side due to electric field induced flux of mobile cations and polar solvent (typically water). IPMCs are one of the most promising EAPs as artificial muscle-like actuators, since they mimic the behavior of biological muscles. IPMCs also exhibit high sensitivity when used as sensors.

Polymer gel actuators [1] can produce larger strains compared to ionic polymer-based actuators. However, they exhibit slower strain response and suffer from low mechanical strength.

Bucky gel actuators are also ionic EAPs, composed of polymer-supported ionic liquid gel layer between two gelatinous electrode layers consisting of ionic liquid and SWCNTs [9, 23]. In terms of actuation dynamics and operating voltage the bucky gel actuators are similar to IPMCs, except they can operate in the air without external electrolytes.

2.2. Potential applications of EAPs

The different types of EAPs mentioned earlier all have numerous potential applications in many technological fields. This chapter briefly introduces the potential applications for ionic type of EAPs.

Ionic EAPs such as ionic polymer-metal composites are attractive for applications that require large bending actuations and low or medium stress. Due to low driving voltage they are primarily suited for applications where high voltage is undesirable.

There are numerous research studies where IPMCs have been exploited as actuators, artificial muscles or sensors in large variety of applications. For instance, IPMC sensors have been investigated as vibration sensors for active noise damping [24]. Examples of other applications where IPMC actuators are used include mechanical grippers, metering valves, and diaphragm pumps [2]. When properly engineered, the bending motion of IPMC can be converted to linear actuation, which can be exploited in variety of robotic manipulators [25].

Due to the unique features, IPMCs have been explored for biomedical and human affinity applications such as active microcatheter, implantable heart-assist device, artificial smooth muscle actuators, surgical tools, peristaltic pumps, and sheet-type braille displays [2, 26].

IPMCs emulate biological muscles and therefore are attractive for development of biologically inspired robots [3, 4]. IPMC actuators have been integrated into many fish-like robotic systems [27, 28], or other aquatic [29] or non-aquatic

bio-inspired systems [30]. In addition to bending actuation, IPMCs with appropriately sectored electrodes can also exhibit twisting type of actuation that can be used as artificial fish-like propulsor to mimic complex motions of real fish fins [31].

2.3. Ionic EAPs

2.3.1. Fabrication methods

Traditional fabrication method

An impregnation-reduction process (often referred to as electroless plating) is the most commonly used method to fabricate ionic polymer-metal composites (IPMCs) [32]. Impregnation reduction method can be implemented for a wide range of ion-exchange polymers (often called ionomers). Ion-exchange polymers contain covalently bonded fixed ionic groups and depending upon the type of material can selectively pass or conduct either cations or anions or both. A popular ion-exchange polymer used as a membrane material for IPMCs is a sulfonated tetrafluoroethylene-based fluoropolymer, i.e. NafionTM (product of DuPont) with covalently fixed SO₃⁻-groups that provide cation-exchange capability. The chemical structure of Nafion is described in Figure 1.

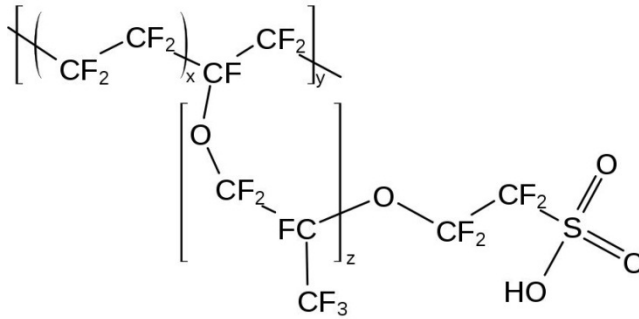
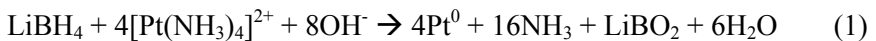


Figure 1. Nafion structure. The hydrogen ion in OH-group can be exchanged.

The impregnation-reduction process involves three main steps. The first step is to impregnate the polymer with appropriate metal salt by soaking it in aqueous metal salt solution such as tetraammineplatinum (II) chloridemonohydrate (Pt(NH₃)₄Cl₂·H₂O) [33]. The metal complex cations diffuse into the membrane via ion-exchange process. The next step is to reduce the platinum complex cations to metallic state on the inner surface of the membrane by soaking the polymer in aqueous solution containing reducing agent such as NaBH₄ or LiBH₄. The reduction of metal salt occurs according to the following reaction:



The described plating cycle is typically repeated multiple times until appropriate electrode thickness and conductivity is achieved. Increasing the number of plating layers enhances the interfacial area and increases the mechanical stiffness that both affect the performance of IPMC. According to Oguro *et al.* [34] the displacement increased with the number of plating cycles and decreased or was steady after five cycles.

The third step is to deposit the metal layer onto the outer surface of the polymer to further increase the conductivity. The membrane is immersed in platinum salt ($\text{Pt}(\text{NH}_3)_4\text{Cl}_2 \cdot \text{H}_2\text{O}$) solution and by adding mild reducing agents such as hydrazine monohydrate and hydroxylamine hydrochloride the metal complex cations are reduced and deposited onto the polymer surface.

The final step is to incorporate desired cations such as Na^+ or Li^+ into the polymer via ion-exchange process by soaking the membrane in respective metal salt solution, e.g. NaCl or LiCl .

Layer-by-layer casting technique

A novel method to simply fabricate so-called ‘dry-type’ ionic liquid containing actuators is by Layer-by-layer casting technique [9]. This actuator has a bi-morph configuration with polymer-supported ionic liquid electrolyte layer sandwiched by bucky gel electrolyte layers. The fabrication process involves preparing a suspension of SWCNTs in 1-butyl-3-methylimidazolium tetrafluoroborate (BMIBF_4) ionic liquid. BMIBF_4 is one of the most widely studied room temperature ionic liquids and has good ionic conductivity and viscosity properties. The suspension is ground in agate mortar to obtain bucky gel that is subsequently transferred to a mixture containing polyvinylidene fluoride-co-hexafluoropropylene ($\text{PVdF}(\text{HFP})$) and 4-methyl-2-pentanone (MP). The mixture is heated at 80 °C for appropriate period, and then the obtained gelatinous material is cast into aluminum mold. The cast is allowed to cool at room temperature to obtain the first electrode layer. Then, a hot gelatinous mixture of ionic liquid and $\text{PVdF}(\text{HFP})$ in MP is cast on top of the first layer. The resultant double layer is allowed to cool to room temperature. Thereafter, the aforementioned hot gelatinous material derived from bucky gel is cast onto the second layer. Finally, the obtained three-layered actuator is allowed to stand in air for overnight and then dried under reduced pressure to remove the volatile solvent (MP). The prepared actuator has a thickness of 0.25–0.3 mm. Such an actuator with built-in ionic liquid can operate in air without external electrolytes at low applied voltages.

Later, following modifications were introduced to this process [23]. The 1-ethyl-3-methylimidazolium tetrafluoroborate (EMIBF_4) ionic liquid was used as an internal electrolyte instead of BMIBF_4 . It was found that EMIBF_4 gives the fastest and largest actuation response among the tested ionic-liquids [35] for the bucky gel actuator. It should be noted that in ambient conditions ionic liquids can absorb some water from the air [36] that may contribute to the actuation. In addition, the mixture of SWCNTs, EMIBF_4 and $\text{PVdF}(\text{HFP})$ in dimethyl-

acetamide was treated by ball-milling. The gelatinous mixture prepared by ball-milling was more homogenous than prepared by grinding in agate mortar used previous method. Further, the electrolyte layer and electrode layers were cast separately and the solvents were completely evaporated. The prepared layers were assembled by hot-pressing to obtain the bucky gel actuator. The actuator thickness was adjusted by pressing appropriate number of electrode layers on both side of the electrolyte layer. A schematic representation of the fabrication process is shown in Figure 2.

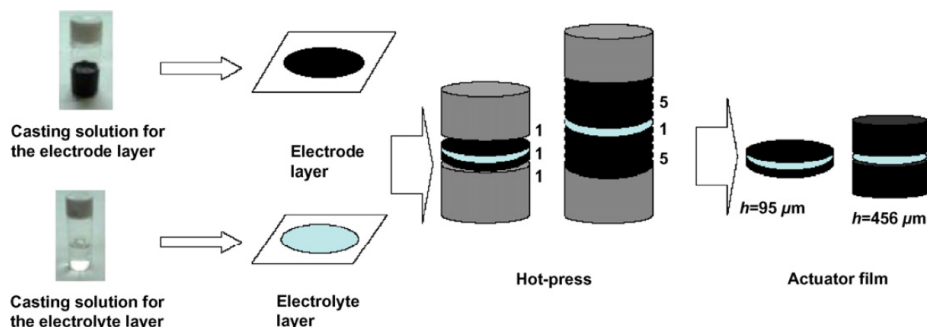


Figure 2. Schematic of the preparation of bucky-gel actuator [23].

Direct Assembly process

Direct Assembly Process offers direct control and flexibility to use various component materials to fabricate actuators. This process can be conducted in two ways, i.e. the electrode is either applied on a dry membrane or solvated membrane [10].

a) Direct assembly process with dry membranes

The ionomer (e.g. Nafion) is first dissolved in an alcohol solution and then mixed with an electrically conductive powder. Additional solvents such as isopropyl alcohol may be added to the mixture to enhance dispersion. The mixture is sonicated for 1–4 h to achieve homogenous dispersion of conductive particles. The obtained conductor-polymer mixture is applied on the polymer in one of two ways. The first method is direct painting of several layers of the mixture on both sides of the membrane using a brush. The sample is dried in an oven at 130 °C for 15 min between each layer. The composite is then hot pressed at 210 °C and a pressure of 20 MPa to conjugate the electrode layers with the membrane. The second approach is to paint several layers of the mixture on a Teflon reinforced glass fabric, and then hot-press the decals on the membrane. After cooling down to room temperature, the membrane is hydrated and the Teflon mesh can be removed.

The electrode conductivity is further increased by impregnation-reduction method or by gold electroplating. A schematic of the fabrication procedure is shown in Figure 3.

Diluents other than water, e.g. formamide, diethylene-glycol or ionic liquids, can be also incorporated into the dry membrane. An issue with such diluents is that they excessively swell the membrane, leading to cracks in the electrode layer. Therefore, the step of increasing the electrode surface conductivity is performed after incorporating the diluent. The composites with low-vapor-pressure solvents can be sandwiched between two gold foils and fused together by a hot-pressing to increase the surface conductivity.

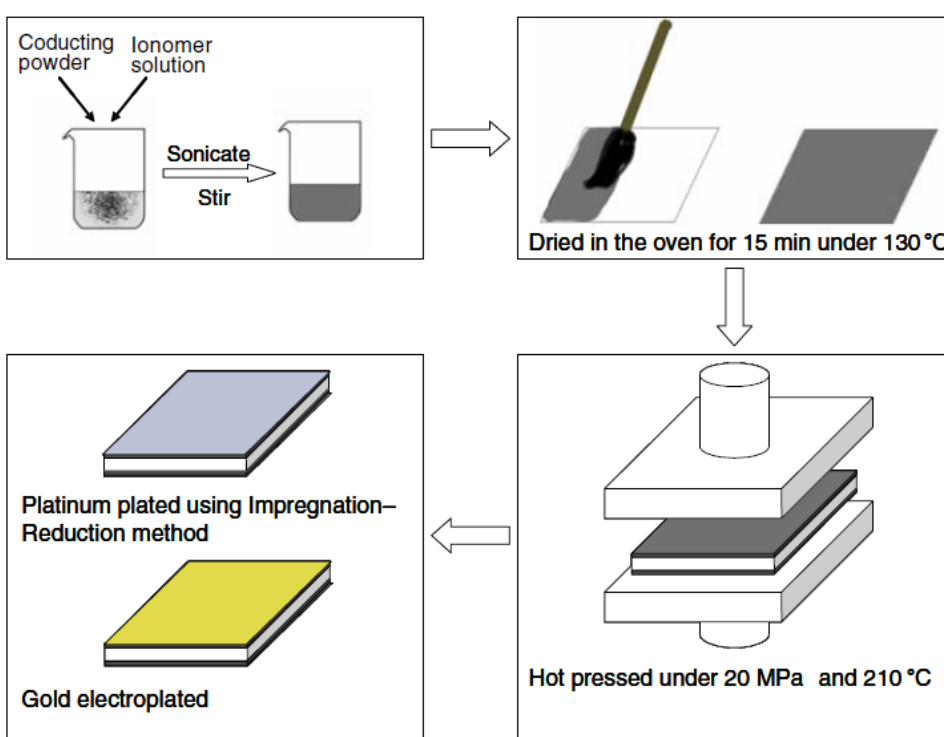


Figure 3. Schematic of the direct assembly process with dry membrane [10].

b) Direct assembly process with solvated membranes

For some diluents, the dry assembly may not be adequate due to excessive swelling of the polymer that leads to delamination of the high surface area electrode. Some diluents may also dissolve the ionomer contained in the electrode layer. In these cases, the Direct Assembly Process is typically conducted on already solvated polymer membranes.

First, the membrane is solvated with proper solvent or electrolyte. Then, the electrode is painted on both surfaces of the membrane and sandwiched between two gold foils and hot-pressed together under appropriate pressure, temperature and duration. A schematic representation of the DAP with solvated membranes is shown in Figure 4. The challenge of this approach is a diluent loss due to evaporation during the hot-pressing. Therefore, dry assembly is preferred for volatile solvents and electrolytes. Depending on diluent the mass loss can be around 30%.

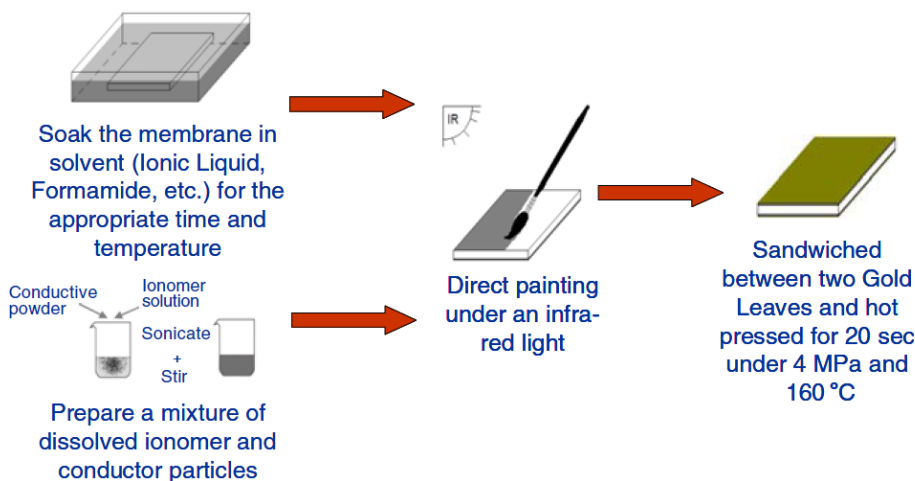


Figure 4. Schematic of the direct assembly process with solvated membrane [10].

2.3.2. Electrode materials

Platinum and gold are commonly used as electrode materials for ionic polymer-metal composites due to their good electrochemical stability and high electrical conductivity [32]. The main disadvantages of these materials are high cost and complex processing. Also, low mechanical stability under cyclic deformations during the actuation has been observed that leads to cracks in the platinum surface and reduces the conductivity that in turn deteriorates the performance [37]. Gold exhibits better mechanical durability, but on the other hand, the high reactivity of the gold complex makes the electroless plating complicated, giving results with low reproducibility. Combination of using platinum and palladium as a supporting layer underneath has shown improved mechanical stability and actuation performance [38]. An alternative electrode composed of platinum and copper has been reported, in which the reversible electrochemical reactions upon the actuation (i.e. dissolution and reduction of Cu^{2+} ions on the inner surfaces of the electrodes) can maintain electrical connections between the cracks of platinum layer [39]. Also, nickel and silver nanopowder have been used as

low-cost electrode materials [40, 41]. However, relatively low electrochemical stability of these materials limits the cycle life of the actuators.

From the mentioned electrode materials, the noble metals are typical choice due to their higher electrochemical stability and availability in cation complex form that can be used applying the impregnation-reduction method. The new manufacturing approaches such as layer-by-layer casting or direct assembly process have broadened the selection of usable materials and opened access for better alternatives.

For instance, RuO_2 or other transition metal oxide (e.g. MnO_2) powders can be effectively used in EAP electrodes [42, 43]. Compared to the noble metals the oxide powders are less expensive and have higher specific surface area (50–60 m^2/g). Metal oxides exhibit fast and reversible redox reactions occurring at the surface of the active material particles. These materials have generally high electrical resistance, therefore metal oxide powders are often used in combination with CNTs, or the metal oxide electrode surface is covered additionally with conductive gold layer.

Carbon nanotubes (esp. single-walled) have received considerable attention as electrode materials in EAP development, due to their high electrical conductivity, good electrochemical stability and relatively high specific surface area (up to 1000 m^2/g) [9, 44–46]. SWCNTs can be simply used either by direct assembly process or layer-by-layer casting technique as described in previous section.

Good alternative materials for EAP electrodes are also highly porous amorphous carbons and carbide-derived carbons, studied in this work. These materials have very high specific surface area (1000–2000 m^2/g), controllable pore structure and high electrochemical stability, and therefore are commonly used in supercapacitors [47–50]. It should be noted that in terms of design and working mechanism the ionic liquid containing EAPs with carbon electrodes are comparable to non-aqueous electrolyte-based capacitors. Also, the driving voltage is comparable to the mentioned capacitors (below 3.5 V). CDCs are produced by extraction of metal ions from carbide lattice via chlorination at elevated temperature [11–14]. Generally, variations in chlorination reaction conditions (extraction time, temperature, after-treatment) lead to variations in pore size, pore volume and specific surface area. The synthesis of CDC is well-controlled, allowing the pore size of the final structure to be fine-tuned with the nanoscale precision [13, 49]. Activated carbons are typically produced by thermal decomposition of organic materials and subsequent activation in water vapor or CO_2 .

Carbon aerogels are promising candidates for EAP electrode materials. Carbon aerogels have large specific surface area and extremely low density compared to single-walled and multi-walled nanoclusters. Therefore, these materials are used as adsorbents, materials for chromatographic separation, and membranes and carriers for metal catalysts. Furthermore, having a controllable porous structure and electrically conductive network, they can be used as

electrodes for supercapacitors [51] or fuel cells [52]. Carbon aerogels used in this study were derived from 5-methylresorcinol-formaldehyde gel [15]. After drying the gel in supercritical carbon dioxide and pyrolyzing in an inert (N_2) atmosphere, the obtained carbon aerogel was ball-milled in order to achieve a fine-powdered material. Activation of these aerogels was conducted at 1173 K in continuous flow of CO_2 for 1–4 hours.

The porous carbon materials also have some shortcomings. Namely, activated carbons and CDCs (prepared at low chlorination temperatures) tend to have poor conductivity within the electrode cross-section [14]. This leads to a slow electrical double layer charging and thus, slower actuation response. There are also structural limitations related to carbon electrodes [11, 12]. It has been pointed out that some activated carbons, although having a high specific surface area, show limited capacitance because of their low attainable microporosity and weak mesoporosity, i.e. poor electrolyte accessibility. To improve actuation performance, CNT electrode additives such as PANI and mesoporous silica were studied by Sugino *et al.* [46]. The combined PANI/CNT electrodes showed a great cycle life and larger tip deflection compared to pure CNT electrodes. Recently, CNTs were used as an additive in activated carbon electrodes of supercapacitors [53]. The CNTs combined with activated carbon powder improved significantly charge storage capacity over the pure CNT electrode and conventional activated carbon electrode.

3. EXPERIMENTAL

The EAP actuators with two different configurations, each fabricated by different method, were studied in this work. In addition, the experimental work was conducted in separate laboratories. Specifically, the EAP actuators composed of ionic polymer membrane (Nafion), conductive powder electrode layers and gold foil on the surface (Figure 5) were fabricated by Direct Assembly Process, and the manufacturing as well as their characterization was performed at IMS Laboratory in Tartu [I–III]. The EAP actuators composed of PVDF-HFP/electrolyte gel layer and SWCNT/CDC electrode layers (Figure 6) were fabricated using so called Layer-by-layer casting technique [IV]. The fabrication and characterization of these actuators was conducted at AIST Research Center in Japan. As a result, the experimental setup and methodology used for characterization of the mentioned actuators obviously varies. Therefore, this section is divided into separate subsections based on fabrication and characterization methods used.

3.1. Fabrication of EAP actuators by Direct Assembly Process

3.1.1. Materials and chemicals used

Ruthenium(IV)oxide powders, hydrous (238058) and anhydrous (40336), were purchased from Sigma-Aldrich and Alfa Aesar, respectively. Carbide-derived carbon (CDC) and coconut shell based activated carbon powders were provided by Tartu Technologies Ltd. The CDC powder was synthesized from TiC precursor by chlorination at 800 °C (noted as CDC TiC-800). The basic procedure for CDC synthesis has been described in [11–14]. Carbon aerogels (activated and non-activated) were prepared as described by Koel et al. [15]. All the electrode materials were used *as received*. Nafion 117 membrane (product of DuPont) was purchased from FuelCellStore.comTM. Gold foil from Gold-Hammer (24-carat, 80x80 mm²) was used as a contact material, hot-pressed onto an electrode surface.

The following reagents were of analytical grade and were used without further purification: 1-ethyl-3-methylimidazolium trifluoromethanesulfonate (EMI-TF, Fluka, 00738); lithium perchlorate (LiClO₄, Fluka); 2-propanol ((CH₃)₂CHOH, 99.9%, Sigma Aldrich); ethanol (CH₃CH₂OH, 96%, SigmaAldrich); hydrochloric acid (HCl, 36%, Stanchem). All solutions were prepared using deionized water (Millipore, Milli-Q).

The physical properties of the electrode materials used are listed in Table 1 and 2.

Table 1. Some properties of carbon materials and RuO₂ powders used.

Electrode material	Density (g/cm ³)	Specific surface area (m ² /g)	Volumetric surface area (m ² /cm ³)	Conductivity (mS/cm)
CDC TiC-800	0.8	1450	1116	~50
Cocunut based activated carbon	0.6	1900	1140	~50
RuO ₂ anhydrous	3.5	55–60	450	N/A
RuO ₂ hydrous	~3.5	< 50	< 400	N/A

Table 2. Some properties of the carbon aerogel powders used.

Electrode material	Density (g/cm ³)	Specific surface area (m ² /g)	Total volume of pores (cm ³ /g)	Average pore width (nm)	Degree of graphitization (%)
Non-activated carbon aerogel	0.42	560	2.07	14.75	0
Activated carbon aerogel	0.59	790	2.18	11.05	0

3.1.2. Preparation of actuator elements

The fabrication of five-layered actuator elements can be divided into three main stages: conditioning of the polymer membrane (surface treatment, cleaning), impregnation of the polymer membrane with an ionic liquid, and fabrication of electrodes by DAP. The details of the process are described in the following.

The both sides of Nafion 117 membrane were roughened with an emery paper (2500 Grit) to remove the top layer of polymer surface, which due to relatively high hydrophobicity interacts weakly with the aqueous solutions used later. The surface roughening also increases the polymer–electrode interfacial area and provides better adhesion with an electrode layer. Both surfaces of the membrane were roughened until the polymer appeared uniformly matte and non-transparent. Then, the membrane was cleaned from impurities by boiling in 1 M hydrochloric acid for 30 minutes, followed by boiling in deionized water for 1 h to remove acid residuals. After replacing the water, the membrane was boiled for an additional 30 min in deionized water.

The procedure for impregnating the polymer with an ionic liquid was as follows: first, the membrane was ion-exchanged to Li⁺-form by boiling in 1 M LiClO₄ aqueous solution for 2 h in order to prevent the degradation of the polymer during relatively long drying procedure at high temperature [42]. After that, the polymer membrane was dried in vacuum oven at 150 °C for 12 h. Thereafter, the membrane was instantly immersed in pure ionic liquid (EMI-TF) and

heated at 150 °C for 5 h. After completion of this procedure, the uptake of EMI-TF is expected to be near 60% of the dry weight of the membrane [43].

As for next step, the Direct Assembly Process [10] was conducted to fabricate the porous electrodes on the ionic liquid-impregnated polymer membrane. A 5 wt% Nafion solution was prepared by heating the Nafion® 1100 ionomer in closed container at 210 °C for 3 h in the presence of a 50% ethanol/water solution while under continuous stirring. Then, the ionomer solution was mixed with conductive powder. For RuO₂ electrodes, the mixture was prepared containing of 6 wt% ruthenium (IV) oxide powder, 47 wt% of Nafion solution (5%) and 47 wt% of isopropanol. The mixture for carbon electrodes was adjusted to contain 1.7 wt% of carbon powder, 48.3 wt% of Nafion solution and 50 wt% of isopropanol. All the prepared mixtures were sonicated from 1 to 3 h to disperse the conductive powder particles homogeneously.

The prepared conductor/ionomer dispersions were directly spray-painted onto the membrane using an airbrush (SB-1107 Sumake) operated by compressed air. Volatile solvents were evaporated under an infrared lamp (150 W, Philips) after spraying of each layer. Typically from 8 to 15 layers of the conductor/ionomer dispersion were sprayed onto both sides of the membrane to achieve the electrode layers with uniform thickness. After painting of the electrodes, a layer of 5 wt% Nafion solution was sprayed on top of the electrode to provide better surface adhesion with the gold foil. Then, the membranes were placed under IR light for an additional 15 min for heat treatment to evaporate excessive solvents. Finally, the membranes were sandwiched between two gold foils (thickness 270 nm) and fused together by hot-pressing at 150 °C under pressure of 3.5 MPa for 5–10 s. This step provides a complete conjugation of electrodes with the membrane and decreases the surface resistance of painted layers to less than 1 Ω/cm, according to the results from the four-point probe measurements.

Using the aforementioned procedures, the EAP actuators with six different electrode materials were assembled (Table 1 and 2): RuO₂ (hydrous and anhydrous), CDC TiC-800, coconut shell-based activated carbon and carbon aerogels (activated and non-activated). The architecture of prepared five-layered EAP actuator is illustrated in Figure 5. All samples were cut into rectangular shapes with dimensions of 40 mm (length) × 8 mm (width).

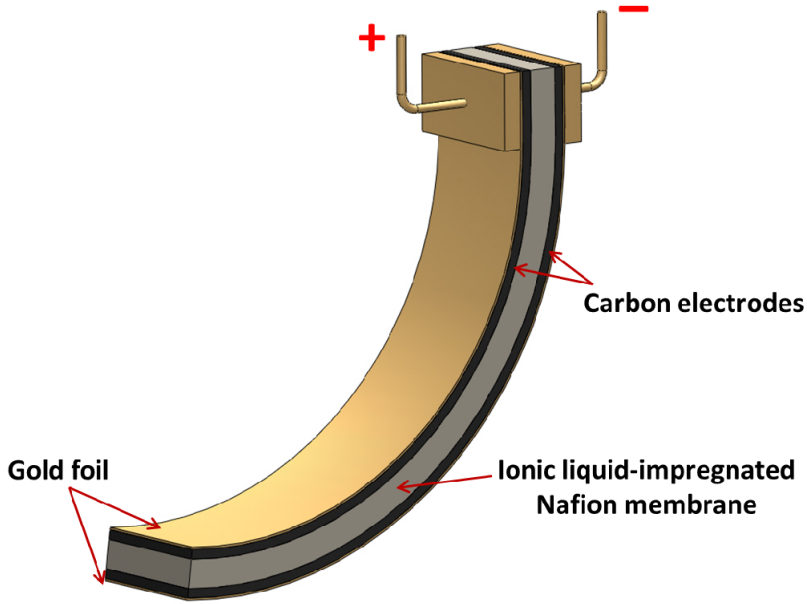


Figure 5. Architecture of five-layered actuator element (in active state).

3.2. Fabrication of EAP acutators by Layer-by-layer casting technique

3.2.1. Materials and chemicals used

The CDC powder, synthesized from TiC precursor via chlorination at 800 °C (noted as CDC-TiC 800), was provided by Tartu Technologies Ltd. The basic procedure for CDC synthesis has been described in [11–14]. CDC TiC-800 has the specific surface area $S_{\text{BET}} = 1470 \text{ m}^2/\text{g}$, total volume of pores $V_{\text{tot}} = 0.71 \text{ cm}^3/\text{g}$, volume of micropores $V_{\text{micro}} = 0.59 \text{ cm}^3/\text{g}$ and average pore size $\text{APS} = 0.97 \text{ nm}$.

The SWCNTs (Purified HiPco®), 1-ethyl-3-methylimidazolium tetrafluoroborate (EMIBF₄), and polyvinylidene fluoride-co-hexafluoropropylene (PVdF(HFP), Kynar Flex^{TRM} 2801) purchased from Unidym. Inc., Fluka, and Arkema Chemicals Inc., respectively, were used as received without further purification. Solvents 4-methyl-2-pentanone (MP) and propylene carbonate (PC) were purchased from Sigma-Aldrich and N,N-dimethylacetamide (DMAc) from Fluka, respectively.

3.2.2. Preparation of actuator elements

The three-layered ionic liquid containing EAP actuator was fabricated from two conductive electrode sheets and a thin polymer/electrolyte gel membrane between them (Figure 6). The actuator electrodes were composed of 20 wt.% of carbon material (either CDC, SWCNTs or mixture of both), 48 wt.% of EMIBF₄, and 32 wt.% of PVdF(HFP). The details for fabrication of the actuator elements by Layer-by-layer casting method are described below.

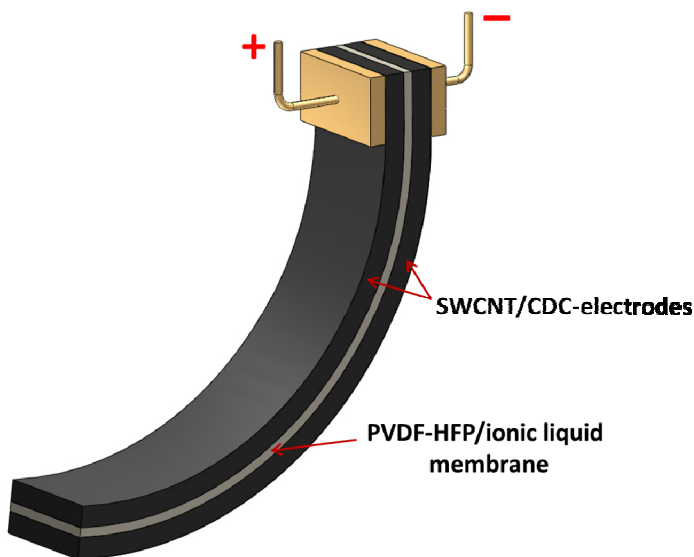


Figure 6. Schematic of the three-layered SWCNT/CDC-actuator (in active state).

A procedure to prepare the electrode layer noted as CDC(100) was the following: 50.2 mg (20 wt.%) of CDC, 80 mg (48.1 wt.%) of PVdF(HFP), and 120 mg (31.9 wt.%) of EMIBF₄ were dissolved in 9 mL of DMAc. The mixture was stirred at the room temperature for 72 h and was further processed in an ultrasonic bath for 24 h. The electrode film was prepared by casting 1.6 mL of CDC suspension into a Teflon mold (with dimensions 2.5 cm × 2.5 cm), and then the cast was heated at 80 °C in a vacuum oven to remove solvent residues. The components of the electrode films for CDC(100), CDC/SWCNT(75/25), CDC/SWCNT(50/50), CDC/SWCNT(25/75) and SWCNT(100) are summarized in Table 3. In each case, the total weight of carbon material (50 mg) was kept constant.

The polymer/electrolyte gel layer was prepared by dissolving 100 mg of EMIBF₄ and 100 mg of PVDF-HFP into mixed solvent of MP (3 mL) and PC (250 mg). Then, 300 µL of the electrolyte solution was casted into an aluminum mold (dimensions 2.5 cm × 2.5 cm) and dried overnight at the room temperature. Thereafter, the solvent was evaporated at 80 °C under reduced pressure for 3 days. The thickness of the electrolyte film varied from 10 to 20 µm.

Table 3. The component ratios of the actuator electrodes.

Actuator notation (wt% of the components in parentheses)	SWCNTs (mg)	CDC (mg)	EMIBF ₄ (mg)	PVdF(HFP) (mg)
CDC(100)	0	50.2	121.1	80.1
SWCNT/CDC(25/75)	12.8	37.6	122.8	80.1
SWCNT/CDC(50/50)	25.3	25.1	122.5	80.5
SWCNT/CDC(75/25)	37.6	12.6	119.7	80.1
SWCNT(100)	50.2	0	121.7	80.4

To obtain a symmetrical three-layered actuator element, the prepared electrolyte film was laminated between two identical electrode films by heat-pressing. The heat-pressing was performed at 70 °C with 10 N (duration 90 s) in first pressing process, then with 270 N (90 s) in second pressing process. The electrode films were conjugated to the electrolyte film during the thermal treatment steps described. Finally, the prepared actuator elements were cut into rectangular shapes with dimensions of 1 mm (width) × 10 mm (length).

3.3. Characterization

3.3.1. EAPs prepared by Direct Assembly Process

Electromechanical and –chemical characterization

A scheme of the experimental setup [7] used for the characterization of the actuator strain, strain rate (speed of bending) and blocking force is shown in Figure 7.

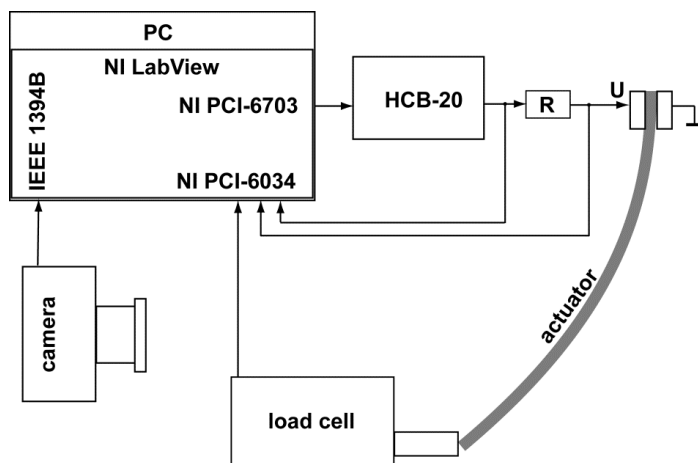


Figure 7. Experimental setup used for electromechanical characterization of EAPs. [II] – Reproduced by permission of The Royal Society of Chemistry.

The actuator was clamped in vertical cantilever position and measurements were performed at ambient temperature and humidity. Square-wave driving pulses were applied via a fixed contact U and a ground contact (gold contacts were used). The measurements were conducted applying National Instruments LabView software. The driving voltage was generated by a NI PCI-6703 DAQ board and amplified by electric current using the high current booster HEKA HCB-20. The voltages with respect to the ground were measured with a NI PCI-6034 DAQ board. The electric input current of the sample was measured as a voltage drop over the resistor R. The value of the resistor was chosen as low as possible, but still sufficiently high with respect to the value of the current and the sensitivity of the measuring equipment. In the course of the experiments described here, the value of the resistor R was from 0.5 to 1.0 Ω . Electric current passed through the sample was calculated according to Ohm's law. A firewire camera (Dragonfly Express, Point Grey Research Inc.) was used for recording the bending motions of the actuator at 30 frames per second. The direction of the camera was set transverse to the actuator and the experiment was illuminated from the background through a frosted glass and a graph paper. In this camera position, the recorded image of the actuator consists of a single curved contrast line. The displacement (δ) of an actuator was determined from the recorded video and was converted to bending strain (ε) using the following well-known equation:

$$\varepsilon = 2\delta W / (L^2 + \delta^2), \quad (2)$$

where L is the free length and W is the thickness of the actuator element [54].

Blocking force was measured at zero displacement using the Panlab MLT0202 load cell. The flexural stiffness of the samples was determined by a three-point bending test [55] as demonstrated in Figure 8.

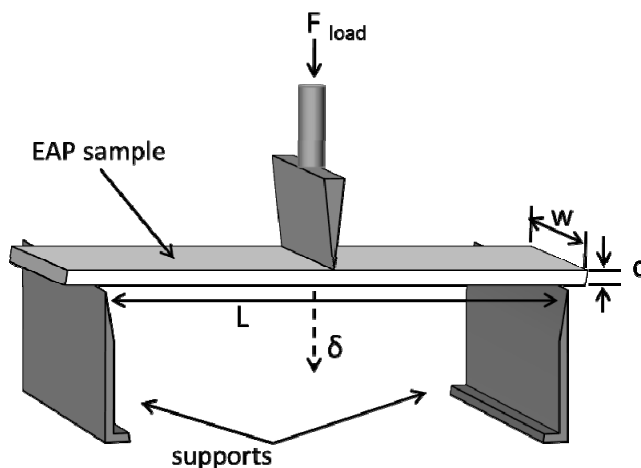


Figure 8. Schematic diagram of the 3-point bending test setup. [II] – Reproduced by permission of The Royal Society of Chemistry.

The Young's modulus was calculated according to equation (3):

$$E = \frac{FL^3}{4\delta wd^3}, \quad (3)$$

where F is applied load, L – length of the beam, δ – displacement, w – width of the sample and d – thickness of the sample.

The electrical resistances (conductivities) of both electrode surfaces were measured by a four-point probe method using a National Instruments PCI-6034 DAQ with a SCC-RTD01 module. The range of the module allows reliable measurement of resistances from 0 to 200 Ω . In order to connect the four probes simultaneously to the actuator strip, a special flexible contact strip was made by fixing four contacts made of gold foil onto the surface of a thin ribbon of PTFE. The distance between the test-contacts was kept at 21 mm. The capacitances of the actuators were determined from the aperiodic charging-discharging curves as described in [56].

SEM

Cross-section scanning electron micrographs (SEM) were obtained for all samples using a Helios Nanolab 600 microscope in secondary electron image mode with a 5 keV accelerating voltage and magnification of 350x. The samples were fractured in liquid nitrogen to obtain clean and flat cross-sectional surface.

Characterization of carbon aerogel materials

The porosity parameters such as Brunauer-Emmett-Teller (BET) surface area, incremental surface area vs. pore width plots, total volume of pores and average pore width for the carbon aerogels were obtained from liquid nitrogen sorption measurements at -196 °C using the Micromeritics ASAP 2020 Surface Area and Porosity Analyzer. An equilibration interval of 5 seconds and low pressure dose of 5.000 cm³/g (at standard pressure and temperature) was used. The degree of graphitization was determined from XRD diffractogram measured by Bruker D8 Advance X-Ray Diffractometer with the Bragg-Brentano geometry and using CuK α radiation ($\lambda=1.54184\text{\AA}$).

3.3.2. EAPs prepared by layer-by-layer casting technique

Electromechanical and –chemical characterization

For displacement measurements one end of an actuator strip was clamped between gold contacts in vertical cantilever position (Figure 9). The dimensions of an actuator element were 1 mm (width) \times 10 mm (length) and the measurements were performed at the ambient temperature and humidity. Hokuto Denko Potentiostat/Galvanostat (HA-501G) with a waveform generator

(Yokogawa Electric FC200) was used to apply an alternating square-wave voltage to the actuator element. The displacement at 5 mm (free length (L)) from the clamp was measured with a laser displacement sensor (Keyence LC2100). The voltage, current, and the displacement were simultaneously recorded with an oscilloscope (Yokogawa DL708). The measured displacement (δ) was converted to the strain (ϵ) according to equation (2).

The cyclic voltammetry was applied to obtain the specific capacitance of the actuator electrodes in a sealed two-electrode cell using a Hokuto Denko HSV-100. Electric conductivity of the electrode film was measured with the four-probe DC current method, using Hokuto Denko Potentiostat/Galvanostat (HA-151) in galvanostatic mode and wave generator (Yokogawa Electric FC220). Tensile stress–strain measurement was carried out to determine the Young's modulus of the electrode film using Seiko Instruments Inc. TMA/SS6000.

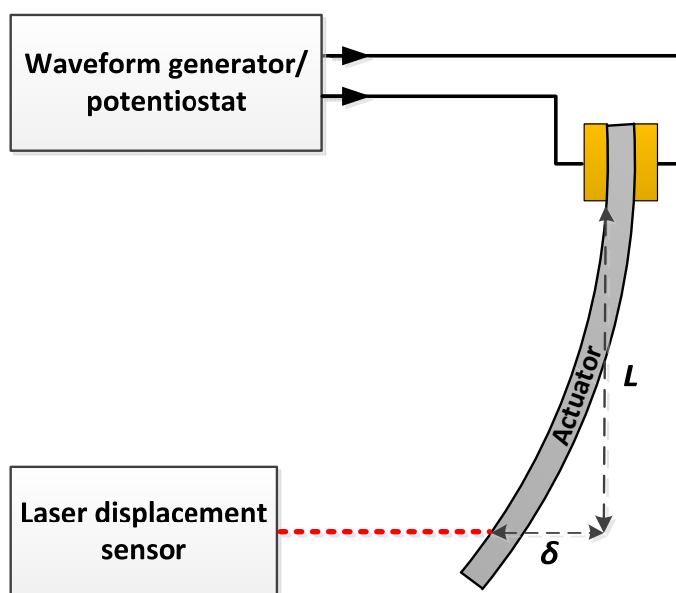


Figure 9. Experimental setup used for actuation measurement of EAPs.

SEM

The cross-section of the actuator elements and morphological changes of the surfaces of electrode films were observed by using SEM (Hitachi TM3000) in secondary electron image mode with 15 keV accelerating voltage at different magnification levels. Samples were quick-frozen in liquid nitrogen and fractured before measurements to get flat and clean surfaces.

4. RESULTS AND DISCUSSION

In Section 4.1., the measured characteristics of the EAP actuators assembled with different electrode materials, including activated carbon, CDC TiC-800, carbon aerogels (activated and non-activated) and RuO₂ (hydrous and anhydrous), are compared and analyzed [I–III]. In Section 4.2., the effects of SWCNT additives in CDC electrodes of the EAP actuators are discussed [IV].

4.1. Comparison of different electrode material properties

The prepared EAP actuators with different electrode materials were evaluated in terms of maximum strain, strain rate, capacitance, electrode surface resistance, blocking force and flexural stiffness (Young's modulus). The cross-sectional morphology of the actuators was examined by SEM. Table 4 represents a summary of the properties measured. The results were obtained by analyzing three EAP samples for each electrode material. For all experiments, the measurement standard deviation percentages were below 15%.

Table 4. A summary of the measured parameters of EAP actuators with different electrodes.

Electrode material	Maximum peak-to-peak strain (%)	Maximum strain rate (%/s)	Capacitance (mF/cm ²)	Electrode surface resistance (Ω /cm)	Blocking force (mN)	Flexural stiffness (MPa)
CDC TiC-800	2.04	0.23	16	0.7	3.6	97
Activated carbon	1.03	0.16	51	0.6	3.1	103
Non-activated carbon aerogel	1.3	0.15	8	0.4	1.7	99
Activated carbon aerogel	1.2	0.13	14	0.3	1	100
RuO ₂ (anhydrous)	0.94	0.09	20	0.6	3.3	88
RuO ₂ (hydrous)	0.69	0.17	36	0.5	3.5	95

SEM

The electrode layer thicknesses and conjugation with the ionic polymer membrane were investigated by observing the cross-sections of the actuator elements by SEM. The cross-sectional images of the samples with different electrode materials are shown in Figure 10. It can be observed that the electrode layer thicknesses on both sides of the membranes are relatively similar, as well

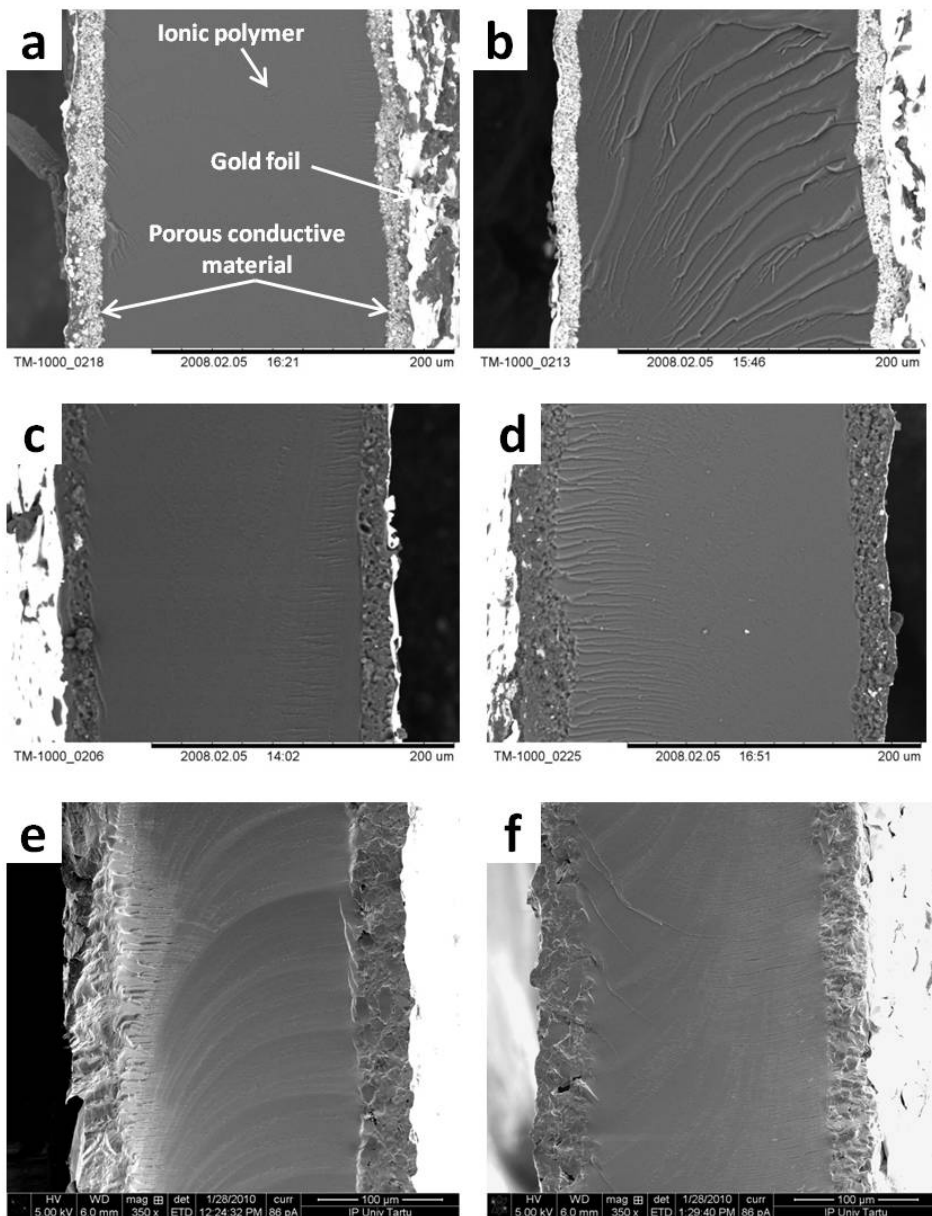


Figure 10. SEM cross-section micrographs of the EAP actuators with different electrodes: a) RuO₂ (hydrous), b) RuO₂ (anhydrous), c) coconut-based activated carbon d) CDC TiC-800, e) activated carbon aerogel, f) non-activated carbon aerogel.

as the thicknesses in the case of different samples. The electrode layer thickness is within the range from 25 to 40 μm and has an average value of 30 μm . The boundary line between the ionic polymer membrane and porous electrode layer is hardly distinguishable, which indicates that the electrodes are well bonded to the polymer membrane. The curved traces and rough areas seen on the polymer and electrode cross-sections are due to fracturing of the samples in liquid nitrogen prior to SEM observations.

Electrode surface resistance

The electrical resistance of the electrode surface was measured in order to make sure that there are no significant cracks or disjunctions in the electrode layer, which are likely to occur during the hot-pressing procedure at elevated temperature. As can be seen from the data in Table 4, the resistance of electrode surface for all the samples are exceptionally low ($< 1 \Omega/\text{cm}$), indicating that the gold foil on the surface was in a good condition, providing good conductivity along the sample length. Very similar values for electrode resistances also assure that the samples can be adequately compared in terms of other characteristics.

Flexural stiffness of the EAP actuators

The flexural stiffness (Young's modulus) of an actuator can strongly affect the electromechanical properties such as bending strain and blocking force. The Young's modulus was determined by the three-point bending test. The data in Table 4 shows that the values of Young's modulus for different samples range from 88–103 MPa, indicating very small variation in flexural stiffness. Thus, the effect of sample's stiffness on other characteristics can be also very minor. The measured data implies that the sample's stiffness is mainly determined by the fabrication process, not by the characteristics of the specific porous electrode material or binding polymer framework properties, which is similar in the samples under study. All the samples were prepared as similarly as possible (i.e. under identical conditions), which explains very minor variations in Young's modulus obtained. For comparison, the stiffness of bare ionic liquid-swollen Nafion membrane was measured. The respective value of Young's modulus was 55 MPa, which indicates that a large portion of sample's stiffness (around 50%) is originated from the electrodes.

Actuation performance

The EAP actuator assembled with CDC electrodes showed by far the highest strain response among the samples, reaching up to 2.04% at ± 2 V square-wave input (Table 4). This exceeds the strain output of RuO_2 (anhydrous) electrodes (used as a reference) by more than twice. The actuator with CDC electrodes also exhibited significantly higher maximum strain rate (up to 0.23% per second), which is nearly 2.5 times higher than that for RuO_2 (anhydrous) electrodes and 35–40% higher compared to RuO_2 (hydrous) and activated carbon electrodes. A large difference in performances between CDC and activated carbon electrodes

is related to their different structures and different pore size distributions. Since the CDC is synthesized by extraction of metal ions from carbide lattice, it has very uniform structure. This well-structured framework facilitates the diffusion of electrolyte ions. Further, the CDC has more uniform pore size distribution – sizes between 0.7 and 0.8 nm, while the activated carbon has wider distribution: 0.6–0.9 nm (determined by Tartu Technologies Ltd). This means that the CDC has greater amount of pores accessible for ionic liquid ions (the size of EMI^+ is $0.71 \times 0.50 \times 0.475$ nm) [57, 58], thereby contributing to higher actuation performance. The actuator with RuO_2 (hydrous) electrodes, on the other hand, showed the lowest strain output, while exhibited higher strain rate compared to RuO_2 (anhydrous) electrodes. The difference between the RuO_2 electrodes can be due to a large particle size and the low porosity of the hydrous material that results in lower specific surface area and therefore, lower strain output. However, sparser structure of RuO_2 (hydrous) electrode might facilitate the electrolyte diffusion, thereby contributing to higher strain rate.

The maximum bending strain for the actuators with non-activated and activated carbon aerogel electrodes were up to 1.3% and 1.2%, respectively. The respective strain rates were 0.15% per second and 0.13% per second. It is interesting to note that although activated carbon aerogel has significantly higher specific surface area compared to non-activated carbon aerogel, the both actuators performed relatively similar in terms of strain output as well as strain rate. The incremental surface area vs. pore width plots (Figure 11) indicate that the activated carbon aerogel, while having almost the same pore structure in bigger micropore range (>1 nm), exhibits considerably higher amount of micropores in the range of 0.5–0.6 nm (sometimes named as nanopores) [49]. The micropores of this size range, however, are probably too small to be quickly accessible for ionic liquid (EMI-TF) ions. Therefore, it can be inferred that the actuation in carbon aerogel-based actuators is mainly generated in bigger micro- and mesopores (2–50 nm) that are freely accessible for electrolyte ions. As observed in Figure 11, both carbons have almost identical incremental surface area vs. pore width data in the micropore range (>1 nm), which explains their very similar performance in strain output and strain rate. It should be noted that the actuator's speed is closely related to the porous structure of electrode, since it directly affects the diffusion rate of electrolyte ions inside the porous electrode matrix.

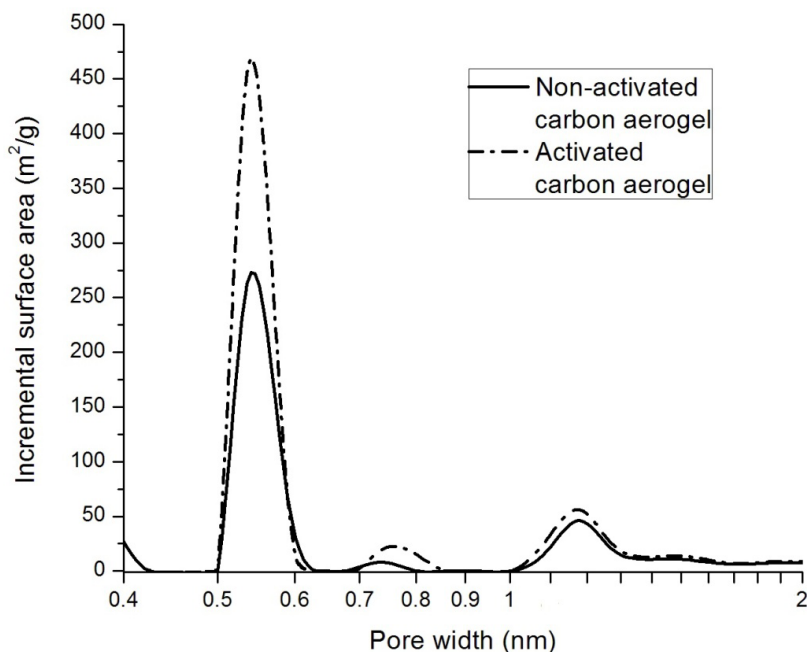


Figure 11. Incremental surface area vs. pore width plots for non-activated and activated carbon aerogels, calculated using non-linear density functional theory [59]. [II] – *Re-produced by permission of The Royal Society of Chemistry.*

The EAP actuators assembled with carbon aerogel electrodes slightly outperformed the maximum strain of activated carbon-based actuator, while showed lower strain response compared to the CDC-based actuator. This is related to the structural differences between the carbon materials. Besides the pore characteristics, the actuation is also affected by the deformability of the carbon particles, which is determined by the degree of graphitization, and can be obtained from XRD data or Raman spectra. In the case of CDC, the degree of graphitization is 5% [60] and it is considered to be intrinsic for carbons with relatively rigid structure. In terms of actuation performance, if the carbon structure is sufficiently rigid and not compressible by the electrostatic interactions during the actuation, the total volume change in electrodes will be greater, which in turn leads to higher strain output. In contrast to the CDC, the degree of graphitization in the case of both carbon aerogels – activated and non-activated – is nearly 0% (Table 2). The reflections (002) and (100) that indicate the graphitization of carbon material were not revealed in the XRD diffractogram for the carbons aerogels (Figure 12). This means that the structures of activated and non-activated carbon aerogels are completely amorphous and hence, significantly more elastic compared to the CDC material. Therefore, during the actuation the structure of carbon aerogels can be compressed in more

extent, thereby diminishing the total volume change in electrodes, which explains lower performance in strain output compared to the CDC. As can be noted in Table 4, carbon aerogels electrodes produced up to 30% more strain compared to the activated carbon electrodes. Unlike the activated carbon, which also has amorphous structure, carbon aerogels exhibit higher pore volume (Table 1). High pore volume refers to the higher content of ionic liquid involved into electrodes, thereby giving rise to higher strain output.

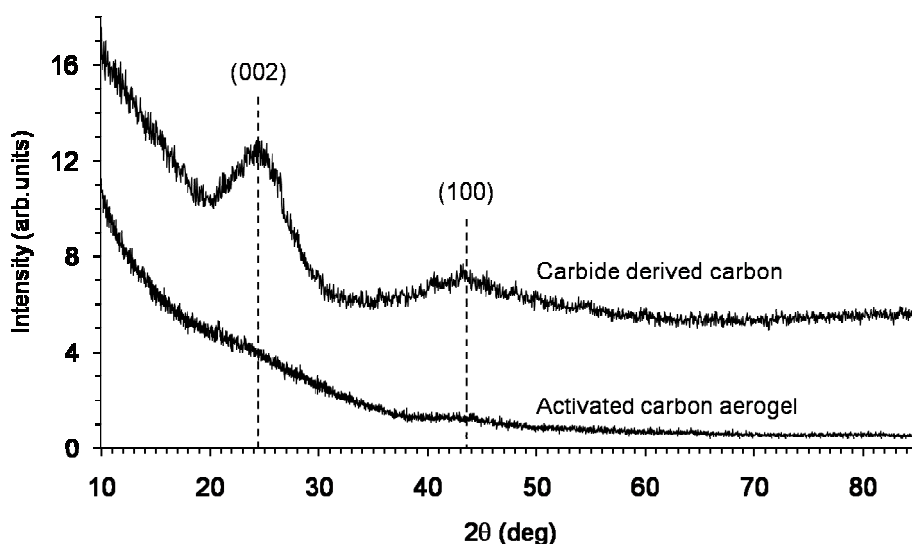


Figure 12. XRD diffractogram of activated carbon aerogel and carbide-derived carbon powders. [II] – *Reproduced by permission of The Royal Society of Chemistry.*

Blocking force

The measured blocking forces for the actuators with CDC and activated carbon electrodes are rather similar, 3.6 mN and 3.1 mN, respectively (Table 4). These results are also very similar to the blocking forces for RuO₂-based actuators. A slight advantage of the CDC electrodes over the activated carbon electrodes is probably related to its higher structural rigidity (explained by higher degree of graphitization). The measurements show that the blocking forces for the actuators with carbon aerogel electrodes are considerably lower compared to the CDC-based actuator. This is most likely due to completely amorphous structure of the both carbon aerogels that is more easily deformable compared to the CDC. Thus, it is clear that the carbon matrix has to be sufficiently rigid in order to generate high force.

Capacitance

An interfacial area between the electrodes and electrolyte can strongly affect the actuation performance (strain output). In this regard, the capacitance measurements were conducted in order to analyze how the specific surface area of electrodes correlates with the strain output. Generally, higher capacitance indicates larger interfacial surface area and more electrolyte ions involved in electrical double layer formation process that in turn refers to a higher strain output due to the stronger electrostatic interactions inside the double layer. However, in the context of the data presented here, the capacitances are not in a good correlation with the respective strain values for the samples tested (Table 4, Figure 13).

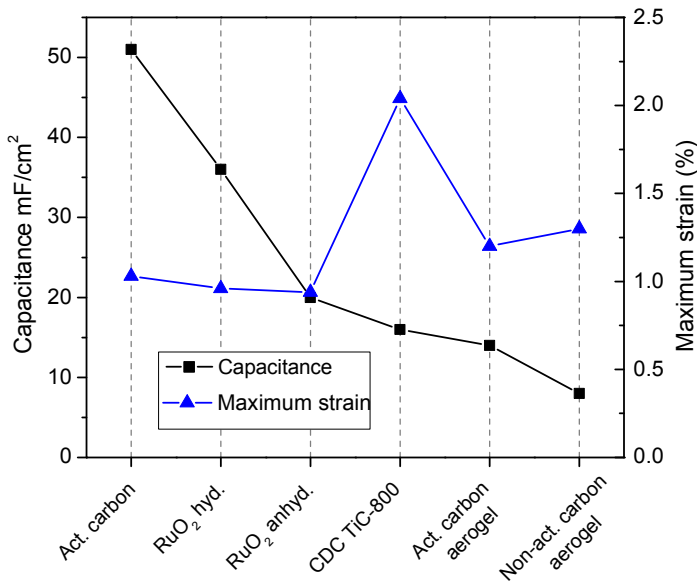


Figure 13. Maximum strain vs. capacitance for the EAPs with different electrode materials.

This is reflected explicitly for the actuator with activated carbon electrodes that exhibited the highest capacitance among the samples (51 mF/m²), but at the same time showed quite moderate actuation performance, remaining around the same level with the strain output of RuO₂ electrodes. These results can be expected, since different electrode materials with different structures are compared. First, the electrode materials studied in this work exhibit different types of capacitances; the carbons have primarily double-layer capacitance, while the RuO₂ powders show significant pseudo-capacitance due to the redox reactions at the electrode surface layers [61]:



The redox processes can increase the value of capacitance up to two orders of magnitude [61]. A typical capacitance for RuO_2 in H_2O is $80 \mu\text{F}/\text{cm}^2$. For the hydrous RuO_2 powder, a capacitance more than $1000 \mu\text{F}/\text{cm}^2$ has been reported [62]. Therefore, it is difficult to compare the strain and capacitance of RuO_2 electrodes with other types of materials. Besides, the strain output is also strongly affected by material-specific structural differences. The differences in capacitances between CDC and activated carbon can be explained by the differences in pore dimensions. The pores in a CDC are almost in the same size as the ions of ionic liquid (EMI^+ has a diameter of 0.71 nm), which can immobilize the ions in the pores and restrict them from penetrating deeper into the electrode structure. Since the porous structure of the electrodes is hardly accessible for the electrolyte ions, the CDC has comparatively low electric double-layer capacitance. However, the ions accumulated into tightly confined pores can more effectively contribute to the volume expansion of carbon matrix during the actuation process and thereby enhance the strain output. On contrary, the pores in activated carbon are large enough for the electrolyte ions to migrate “freely” into the electrode matrix, which explain the larger capacitance compared to CDC. However, the resultant volume effect induced in the electrodes during the actuation process also depends on the rigidity of carbon structure, i.e. on the degree of graphitization. The activated carbon is completely amorphous (degree of graphitization 0%) and significantly softer than the CDC structure (graphitization degree nearly 5%). Therefore, in activated carbon the internal stresses initiated by the electrostatic repulsions during the actuation can be dissipated in compression of the structure, which results in lower strain output compared to the CDC.

Also, it is interesting to note that the actuator with non-activated carbon aerogel electrodes, despite having slightly higher strain performance, showed considerably lower capacitance ($8 \text{ mF}/\text{cm}^2$) compared to the activated carbon aerogel electrodes ($14 \text{ mF}/\text{cm}^2$). As discussed earlier, the activated carbon aerogel has significantly higher amount of smaller micropores ($<1 \text{ nm}$) compared to that for the nonactivated carbon aerogel (Figure 11). Although these micropores are too small to be quickly penetrable for electrolyte ions, they may still contain adsorbed electrolyte ions that are slowly mobile. Based on the impedance spectroscopy data the differential capacitance for CDC|ionic liquid interface can be divided into three parts: so called low frequency capacitance ($\omega \rightarrow 0$), medium frequency capacitance ($10 \text{ mHz} < \omega < 10 \text{ kHz}$) and high frequency capacitance ($\omega \rightarrow \infty$), so-called double layer capacitance for macroscopically ideally flat electrode (ω is the AC angular frequency) [57, 58]. These adsorbed slowly mobile ions are not contributing to the actuation process, but still give rise to the capacitance, which explains the higher capacitance for activated carbon aerogel electrodes, while having slightly lower bending performance compared to the non-activated carbon aerogel electrodes.

4.2. Effects of carbon nanotube additives in carbide-derived carbon electrodes

The SWCNT/CDC-actuators with five different electrode compositions were characterized in terms of frequency dependent strain output, maximum stress, stiffness (Young's modulus), electrode conductivity, charge consumption, and electrical capacitance. The measured parameters are summarized in Table 5. The SEM micrographs of the electrode cross-sections for three different SWCNT/CDC ratios are shown in Figure 14. It can be observed from the images that SWCNT/CDC(25/75) electrode structure (Figure 14a) contains more CDC grains compared to SWCNT/CDC(50/50) (Figure 14b). Similarly, the cross-section of SWCNT/CDC(50/50) shows more CDC grains compared to SWCNT/CDC(75/25) electrode (Figure 14c).

Table 5. The measured characteristics of SWCNT/CDC-actuators with different composition.

Actuator notation (wt% of the electrode components in parentheses)	Maximum strain (%)	Stress at max. strain (MPa)	Young's modulus (MPa)	Electrode conductivity (S/cm)	Specific capa- cittance at 1 mV/s scan rate (F/g)
SWCNT(100)	0.587	1.57	268	2.42	38.2
SWCNT/CDC(75/25)	0.514	0.89	173	0.93	73.8
SWCNT/CDC(50/50)	0.851	1.38	162	0.3	97.9
SWCNT/CDC(25/75)	0.595	0.89	149	0.19	94.8
CDC(100)	0.345	0.11	32	0.16	119.8

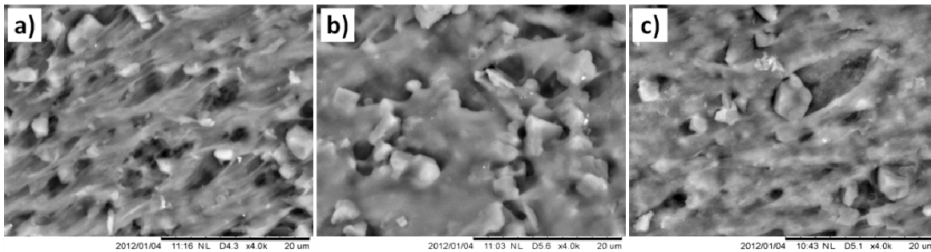


Figure 14. SEM images of the electrode cross-sections at 4000 × magnification: (a) SWCNT/CDC(25/75), (b) SWCNT/CDC(50/50) and (c) SWCNT/CDC(75/25) electrode.

The actuation performance (strain output) of the EAP actuators was examined as function of frequency between 5 mHz–200 Hz at ± 2 V square wave input (Figure 15). It can be observed that all the samples performed very similarly

above 50 Hz, however, the variation in strain performance was significant below 50 Hz (Figure 15c). The strain of the SWCNT(100)-actuator increased rapidly and reached up to 0.11% at 5 Hz, while the strain of the CDC(100)-actuator remained relatively unchanged and was only around 0.005% at 5 Hz. A large difference in the performance of these two actuators between 50 Hz–5 Hz can be attributed entirely to the mesoporous structure of the pure SWCNT electrodes and nearly 15 times higher electrode conductivity compared to the pure CDC electrodes (Figure 16). Although microporous CDC electrodes showed significantly higher specific capacitance when measured at low potential scan rate (1 mV/s) (Table 5), the charge accumulation monitored during the actuation showed that the SWCNT electrodes are able to consume considerably more charge, especially at the higher frequencies (Figure 17). Hence, it can be inferred that the actuation performance at higher frequencies is largely determined by the electrode conductivity and accessibility of electrolyte ions into the porous surface layer of the electrodes. Even though the specific surface area of SWCNTs is relatively low compared to CDC, more importantly, it is quickly accessible for ions participating in EDL formation at higher charging rates. Micropores in CDC are tightly packed and therefore harder to reach at higher charging rates. It should be noted that before mounting the sealed two-electrode cell the SWCNT/CDC electrodes and electrolyte layer were kept in ambient conditions and were not vacuumed before measurements. The contamination of water in CV measurements should be at same level as for actuator elements in strain measurements. However, during cycling the electrode material was isolated from ambient conditions. Therefore, the exact comparison of the strain of the actuator in ambient conditions to the specific capacitance measurements is a bit complicated. The ionic liquid as well as porous electrode will take some water which can contribute somewhat to the actuation process at higher square wave voltages (above 1.23 V).

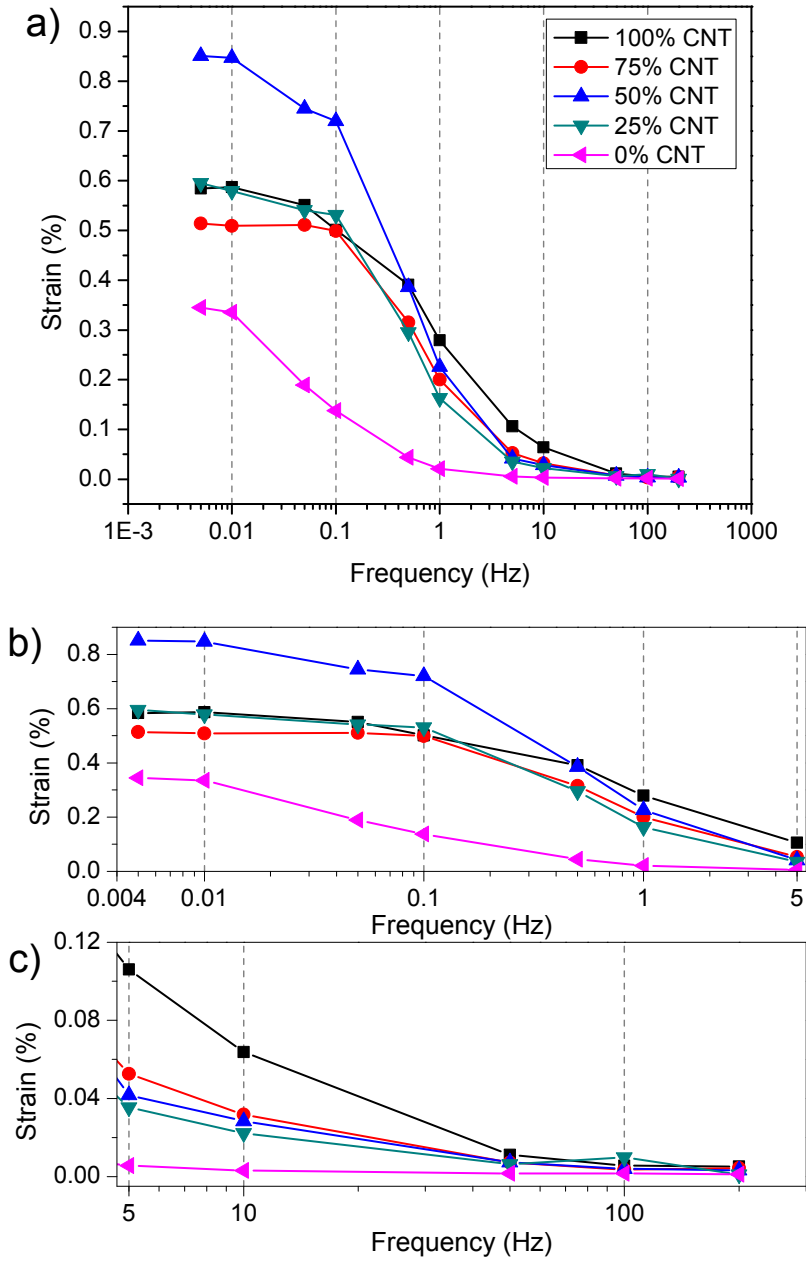


Figure 15. The strain output of the actuators as function of frequency between 5 mHz–200 Hz (a), and detailed views of lower frequency range (5 mHz–5 Hz) (b) and higher frequency range (5 Hz–200 Hz) (c), measured at ± 2 V square wave input.

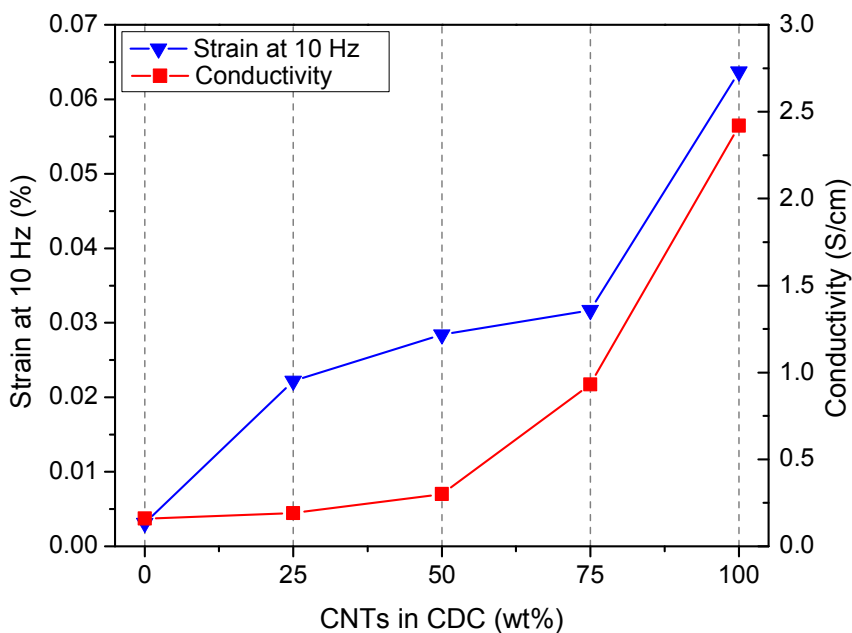


Figure 16. Bending strain of the actuators (at 10 Hz) and electrode conductivities with respect to the content of SWCNTs in electrodes.

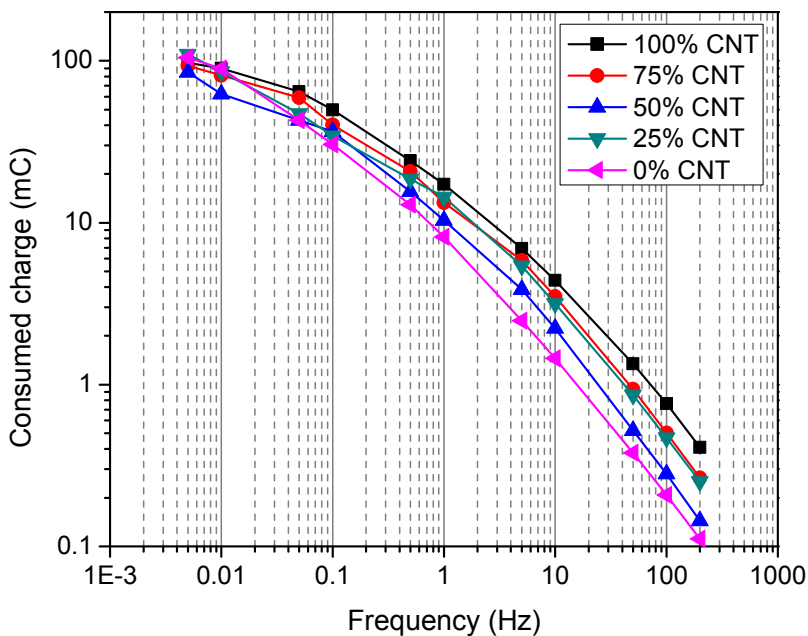


Figure 17. Charge consumption of the actuators as a function of actuation frequency between 5 mHz–200 Hz at ± 2 V square wave input.

The EAP actuators containing 25%, 50% and 75% of SWCNTs in the electrodes revealed somewhat higher strain response compared to the CDC(100)-actuator, but did not reach the strain output of the SWCNT(100)-actuator (Figure 15c). It can be noted that these results are in a good correlation with electrode conductivities (Figure 16), Young's modulus (Figure 18), and specific capacitances of the actuators (Table 5). Relatively minor differences in performances of the SWCNT/CDC(25/75), SWCNT/CDC(50/50) and SWCNT/CDC(75/25) actuators at higher frequencies are related to rather small differences in the mentioned characteristics. It should be noted that higher capacitance is typically associated to higher strain output if actuators with the same electrode structures are compared. In the case of the actuators presented here, the electrode structures of each actuator are different, i.e. the mesoporosity in electrodes is increased by increasing the content of SWCNTs, which enhances the rate of the electrolyte mass transfer (diffusion), thereby contributing to the faster strain response. Considering that the specific capacitance measured at sufficiently low potential scan rate (1 mV/s) involves adsorption into both micro- and mesoporous surfaces, it can be concluded that the capacitances of the actuators are nearly proportional to the microporosity (content of CDC) and inversely proportional to the mesoporosity (content of SWCNTs) in the electrodes. Therefore, an inverse correlation between the strain and capacitance is expected.

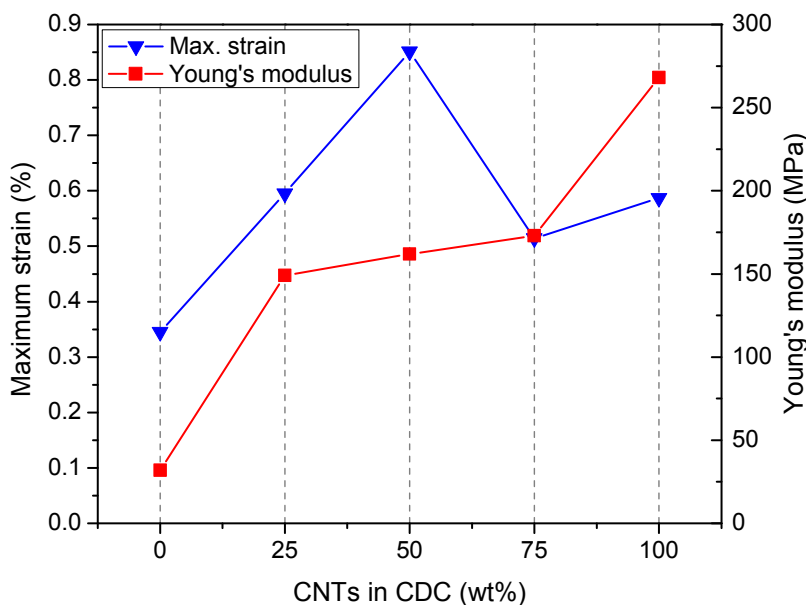


Figure 18. Maximum strain output and Young's modules of the actuators with respect to the content of SWCNTs in electrodes.

Interestingly, the SWCNT/CDC(50/50)-actuator, which showed an average performance at the higher frequency range, displayed by far more strain output at the lower frequencies (< 0.5 Hz) compared to other EAP samples. The strain output increased rapidly up to 0.72% at 0.1 Hz and achieved the plateau at 0.01 Hz with maximum strain of 0.85% (Figure 15b). Compared to the pure CDC-based EAPs with maximum strain of approximately 0.35%, the improvement in the actuation was more than twice. The distinctively superior performance for SWCNT/CDC(50/50) electrodes can be observed explicitly in Figure 19, where the strain outputs of the actuators at 1 Hz, 0.5 Hz and 0.01 Hz are plotted with respect to the content of SWCNTs in their electrodes. It is also interesting to note that the actuator based on pure SWCNT electrodes that showed the highest strain output at higher frequencies performed very similarly to the SWCNT/CDC(25/75) actuator. These results can be explained by a combined effect of the actuator's stiffness (Young's modulus) and specific capacitance acting on the bending strain at the lower frequency range. It should be noted that at lower actuation frequencies the charging times are sufficiently long such that electrolyte ions are able to migrate into hardly accessible micropores. This can be inferred from the fact that the bending strains of all the samples, including the microporous CDC(100), reach the plateau at lower frequencies (Figure 15b),

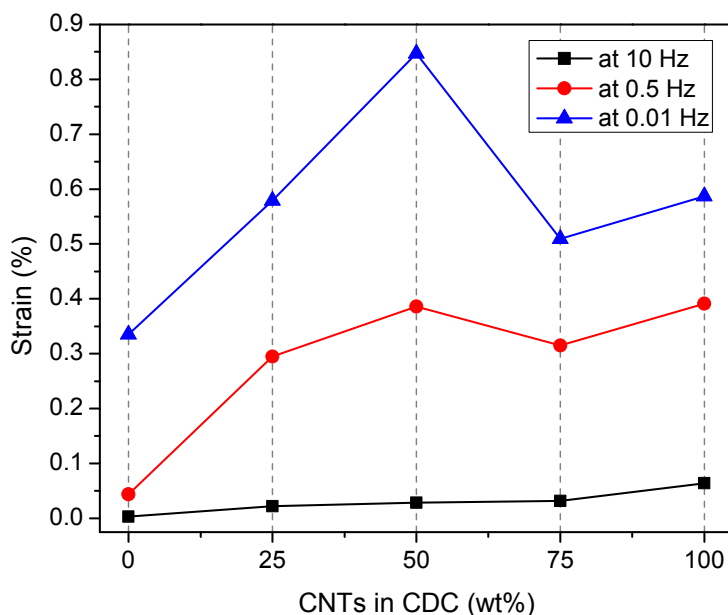


Figure 19. Bending strain output of the actuators at 10 Hz, 0.5 Hz and 0.01 Hz under ± 2 V square wave input with respect to the content of SWCNTs in electrode.

indicating equilibrium adsorption of the electrolyte ions into the porous surface of the electrodes. The specific capacitance that characterizes adsorption equilibrium on both micro- and mesoporous surface, is therefore the determining factor in the actuation process. However, the relation between the strain and capacitance is not as straightforward, since the samples contain different amounts of SWCNTs, which affect both the mesoporosity and the stiffness of the actuators.

As mentioned earlier, the structural deformability of the carbon matrix can significantly impact the maximum strain output of the actuator. Carbon electrodes with higher rigidity tend to be less compressible under the internal stresses that are induced by the electrostatic interactions during the electrical double-layer formation step. Therefore, the total volume change of the electrodes (and thus the bending strain) can be higher compared to more elastic electrodes. In case of soft carbon (activated carbons, carbon aerogels) based electrodes the volume expansion initiated by the electrostatic effects can be absorbed and dissipated during the compression of the carbon matrix, resulting in less strain output. As can be observed, the stiffness of the actuators increases with the content of SWCNTs (Figure 18), whereas the specific capacitance increases with the content of CDC in the electrodes (Table 5). It was found that at the lower frequency range the mentioned parameters are related to the bending strain (ε) as follows:

$$\frac{1}{\varepsilon} = \frac{A}{Y_e} + \frac{B}{C_m}, \quad (5)$$

where Y_e is the Young's modulus and C_m is the specific capacitance of the actuator material, and A and B are constants with the values of 80 MPa and 80 F/g, respectively. Figure 20 shows that this relation fits the experimental strain values reasonably well. Based on the aforementioned data, it can be concluded that the superior actuation performance from the SWCNT/CDC(50/50)-actuator is due to the well balanced combination of elasticity and proper ratio of micro- and mesoporosity in the electrodes.

The actuation performance of the EAP samples was also evaluated in terms of stress (bending force), and was calculated from Young's modulus and maximum bending strain values. As demonstrated in Figure 21, the addition of SWCNTs into the EAP electrodes improved significantly the generated stress of the actuators. The SWCNT(100)-actuator exhibited the highest stress (1.57 MPa), which is due to its moderate strain and very high Young's modulus compared to the other samples studied in this work. However, the SWCNT/CDC(50/50) electrodes clearly offer the best combination in terms of stress and maximum strain output.

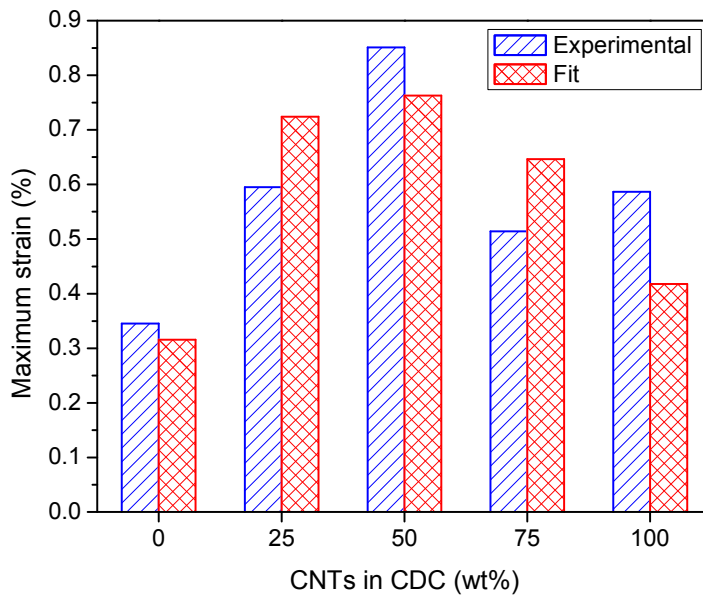


Figure 20. Maximum bending strain of the actuators fitted according to equation (5).

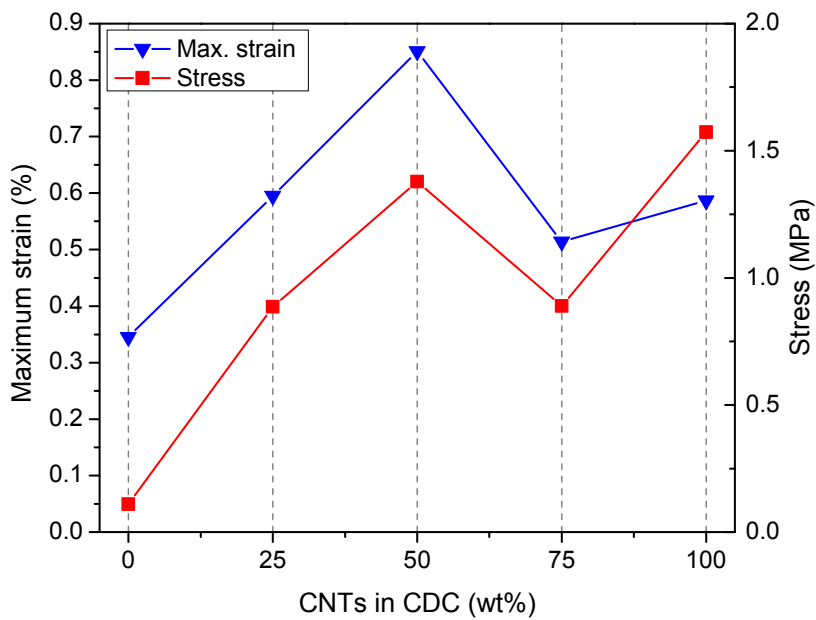


Figure 21. Maximum strain output and generated stress of the actuators with respect to the content of SWCNTs in electrodes.

5. SUMMARY

Carbide-derived carbon (CDC), coconut shell-based activated carbon, and carbon aerogel powders (activated and non-activated) were investigated as new alternative materials for application in electroactive polymer (EAP) actuator electrodes. The respective electrode materials were tested in five-layered actuator systems composed of 1-ethyl-3-methylimidazolium trifluoromethanesulfonate (EMI-TF)-impregnated Nafion membrane between two carbon electrode layers and gold foil on the surface. The electromechanical, electrochemical and mechanical characteristics of the prepared EAP actuators were examined and compared to the actuators based on both hydrous and anhydrous RuO₂ electrodes.

The EAP actuator assembled with carbide-derived carbon electrodes produced the highest bending strain among the samples, up to 2.04% at ± 2 V square-wave input, exceeding the strain of anhydrous RuO₂ electrodes by more than twice. The CDC electrodes also exhibited significantly higher maximum strain rate, up to 0.23% per second, which is nearly 2.5 times higher than measured from samples with RuO₂ (anhydrous) electrodes. The electrodes made of activated carbon performed rather similarly to the RuO₂-based actuators. The maximum bending strain for EAPs with non-activated and activated carbon aerogel electrodes were up to 1.3% and 1.2%, respectively. The respective strain rates were 0.15% per second and 0.13% per second.

The detailed analysis of the measured data indicates that the actuation performance of the EAPs is strongly affected by the porosity parameters and structural rigidity (degree of graphitization) of the carbon electrode materials.

The superior performance of the CDC electrodes can be mainly attributed to high degree of graphitization (5%) and high specific area in micropore range (0.7–0.8 nm) that matches closely with the dimensions of the electrolyte (EMI-TF) ions. Both of these properties contribute to the larger volume expansion effect generated in electrodes during the actuation process. The low temperature N₂-sorption measurements showed that activated and non-activated carbon aerogels have almost identical pore structure within micropore range, which explains minor differences in their actuation performance. Although activated carbon aerogel has higher specific area within the smaller micropore range (0.5–0.6 nm), the pores in this size range are too small to be quickly accessible for the electrolyte ions. The XRD analysis showed that the carbon aerogels (activated and non-activated) have completely amorphous structure (degree of graphitization 0%), and as a result, are considerably softer and more elastic compared to CDC, which has measurable graphitization level and microscopic graphitic areas. Therefore, inside carbon aerogel electrodes the internal stresses initiated from the electrostatic interactions during the actuation can be dissipated in compression of the carbon matrix that results in lower strain output compared to that for the CDC based EAPs.

The effects of single-walled carbon nanotube (SWCNT) additives on the actuation performance were investigated in three-layered actuator systems composed of polyvinylidene fluoride-co-hexafluoropropylene (PVdF(HFP) and 1-ethyl-3-methylimidazolium tetrafluoroborate (EMIBF₄) electrolyte layer between two SWCNT/CDC electrode layers. The actuators were assembled with five different ratios of SWCNTs to CDC in the electrodes and their electro-mechanical, electrochemical and mechanical properties were comparatively analyzed. Analysis of the measured data demonstrates that the increase of the content of SWCNTs in the composite electrodes increased considerably the conductivity of electrodes and the stiffness (Young's modulus) of the actuators. The addition of SWCNTs into the electrodes improved significantly the bending strain output. At higher actuation frequencies (0.5–50 Hz) the improvement can be mainly attributed to enhanced electrode conductivity and increased mesoporosity, i.e. quicker and higher electrolyte ion accessibility into porous matrix of electrodes. At low frequency range (5 mHz–0.5 Hz), the SWCNT/ CDC (50/50)-actuator showed by far the highest bending strain among the tested samples (up to 0.85%), which compared to the pure CDC electrodes with maximum strain of 0.35% is an improvement of more than two times. The SWCNT/CDC (50/50)-actuator also showed the best combination in terms of stress (bending force) and maximum strain output. A strong co-effect of the specific capacitance and Young's modulus on the bending strain was observed at the lower frequency range. A correlation between the mentioned parameters derived indicates that the superior performance of SWCNT/CDC (50/50) electrodes is due to a unique ratio of micro- and mesoporosity inside the EAP electrodes combined with moderately high stiffness of carbon matrix.

6. REFERENCES

- [1] Y. Bar-Cohen, *Electroactive polymer (EAP) actuators as artificial muscles : reality, potential, and challenges*, 2nd ed., SPIE Press, Bellingham, Wash., 2004.
- [2] M. Shahinpoor, K.J. Kim, *Ionic polymer-metal composites: IV. Industrial and medical applications*, *Smart Materials & Structures* 14 (2005) 197–214.
- [3] Y. Bar-Cohen, *Biomimetics using electroactive polymers (EAP) as artificial muscles - A review*, *Journal of Advanced Materials* 38 (2006) 3–9.
- [4] Y. Bar-Cohen, *Biomimetics: biologically inspired technologies*, CRC Press, Boca Raton, FL, 2006.
- [5] K. Oguro, Y. Kawami, H. Takenaka, *Bending of an ion-conducting polymer film-electrode composite by an electric stimulus at low voltage*, *Journal of Micromachine Society* 5 (1992) 27–30.
- [6] M. Shahinpoor, Y. Bar-Cohen, J.O. Simpson, J. Smith, *Ionic polymer-metal composites (IPMCs) as biomimetic sensors, actuators and artificial muscles - a review*, *Smart Materials & Structures* 7 (1998) R15-R30.
- [7] A. Punning, M. Kruusmaa, A. Aabloo, *A self-sensing ion conducting polymer metal composite (IPMC) actuator*, *Sensors and Actuators a-Physical* 136 (2007) 656–664.
- [8] V. Palmre, S.J. Kim, K. Kim, *Millimeter thick ionic polymer membrane-based IPMCs with bimetallic Pd-Pt electrodes*, in: Y. Bar-Cohen, F. Carpi (Eds), 1 ed., SPIE, San Diego, California, USA, 2011, pp. 797615 (2011).
- [9] T. Fukushima, K. Asaka, A. Kosaka, T. Aida, *Fully plastic actuator through layer-by-layer casting with ionic-liquid-based bucky gel*, *Angewandte Chemie-International Edition* 44 (2005) 2410–3.
- [10] B.J. Akle, M.D. Bennett, D.J. Leo, K.B. Wiles, J.E. McGrath, *Direct assembly process: a novel fabrication technique for large strain ionic polymer transducers*, *Journal of Materials Science* 42 (2007) 7031–41.
- [11] A. Jänes, E. Lust, *Electrochemical characteristics of nanoporous carbide-derived carbon materials in various nonaqueous electrolyte solutions*, *Journal of the Electrochemical Society* 153 (2006) A113-A6.
- [12] I. Tallo, T. Thomberg, K. Kontturi, A. Jänes, E. Lust, *Nanostructured carbide-derived carbon synthesized by chlorination of tungsten carbide*, *Carbon* 49 (2011) 4427–33.
- [13] V. Presser, M. Heon, Y. Gogotsi, *Carbide-Derived Carbons – From Porous Networks to Nanotubes and Graphene*, *Advanced Functional Materials* 21 (2011) 810–33.
- [14] T. Thomberg, A. Jänes, E. Lust, *Energy and power performance of electrochemical double-layer capacitors based on molybdenum carbide derived carbon*, *Electrochimica Acta* 55 (2010) 3138–43.
- [15] F. Perez-Caballero, A.L. Peikolainen, M. Uibu, R. Kuusik, O. Volobujeva, M. Koel, *Preparation of carbon aerogels from 5-methylresorcinol-formaldehyde gels*, *Microporous and Mesoporous Materials* 108 (2008) 230–6.
- [16] L. Seminara, M. Capurro, P. Cirillo, G. Cannata, M. Valle, *Electromechanical characterization of piezoelectric PVDF polymer films for tactile sensors in robotics applications*, *Sensors and Actuators A: Physical* 169 (2011) 49–58.
- [17] J.D.W. Madden, *Chapter 2 – Dielectric elastomers as high-performance electroactive polymers*, in: F. Capri, D. Rossi, R. Kornbluh, R. Pelrine, P. Sommer-

- Larsen A2 – F. Carpi, P. Sommer-Larsen (Eds), *Dielectric Elastomers as Electro-mechanical Transducers*, Elsevier, Amsterdam, 2008, pp. 13–21.
- [18] R. Pelrine, R. Kornbluh, Q. Pei, J. Joseph, High-Speed Electrically Actuated Elastomers with Strain Greater Than 100%, *Science* 287 (2000) 836–9.
 - [19] T. Xie, Tunable polymer multi-shape memory effect, *Nature* 464 (2010) 267–70.
 - [20] E. Smela, W. Lu, B.R. Mattes, Polyaniline actuators: Part 1. PANI(AMPS) in HCl, *Synthetic Metals* 151 (2005) 25–42.
 - [21] H. Gao, J. Zhang, W. Yu, Y. Li, S. Zhu, Y. Li, T. Wang, B. Yang, Monolithic polyaniline/polyvinyl alcohol nanocomposite actuators with tunable stimuli-responsive properties, *Sensors and Actuators B: Chemical* 145 (2010) 839–46.
 - [22] U.L. Zainudeen, M.A. Careem, S. Skaarup, PEDOT and PPy conducting polymer bilayer and trilayer actuators, *Sensors and Actuators B: Chemical* 134 (2008) 467–70.
 - [23] K. Mukai, K. Asaka, K. Kiyohara, T. Sugino, I. Takeuchi, T. Fukushima, T. Aida, High performance fully plastic actuator based on ionic-liquid-based bucky gel, *Electrochimica Acta* 53 (2008) 5555–62.
 - [24] D. Bandyopadhyay, B. Bhattacharya, A. Dutta, An active vibration control strategy for a flexible link using distributed ionic polymer metal composites, *Smart Materials and Structures* 16 (2007) 617.
 - [25] M. Yamakita, N. Kamamichi, Y. Kaneda, K. Asaka, Z.W. Luo, Development of an artificial muscle linear actuator using ionic polymer-metal composites, *Advanced Robotics* 18 (2004) 383–99.
 - [26] K. Yusaku, S. Tsuyoshi, T. Makoto, D. Masao, A. Kinji, S. Takayasu, S. Takao, Sheet-Type Braille Displays by Integrating Organic Field-Effect Transistors and Polymeric Actuators, *Electron Devices, IEEE Transactions on* 54 (2007) 202–9.
 - [27] M. Aureli, V. Kopman, M. Porfiri, Free-Locomotion of Underwater Vehicles Actuated by Ionic Polymer Metal Composites, *Mechatronics, IEEE/ASME Transactions on* 15 (2010) 603–14.
 - [28] S.-W. Yeom, I.-K. Oh, A biomimetic jellyfish robot based on ionic polymer metal composite actuators, *Smart Materials and Structures* 18 (2009) 085002.
 - [29] G. Shuxiang, S. Liwei, K. Asaka, IPMC actuator-based an underwater microrobot with 8 legs, *Mechatronics and Automation, 2008. ICMA 2008. IEEE International Conference on*, 2008, pp. 551–6.
 - [30] M. Yamakita, N. Kamamichi, T. Kozuki, K. Asaka, L. Zhi-Wei, Control of Biped Walking Robot with IPMC Linear Actuator, *Advanced Intelligent Mechatronics. Proceedings, 2005 IEEE/ASME International Conference on*, 2005, pp. 48–53.
 - [31] J.J. Hubbard, M. Fleming, K.K. Leang, V. Palmre, D. Pugal, K.J. Kim, Characterization of Sectored-Electrode IPMC-Based Propulsors for Underwater Locomotion, *ASME Conference Proceedings 2011* (2011) 171–80.
 - [32] M. Shahinpoor, K.J. Kim, Ionic polymer-metal composites: I. Fundamentals, *Smart Materials & Structures* 10 (2001) 819–33.
 - [33] K.J. Kim, M. Shahinpoor, Ionic polymer-metal composites: II. Manufacturing techniques, *Smart Materials & Structures* 12 (2003) 65–79.
 - [34] K. Oguro, N. Fujiwara, K. Asaka, K. Onishi, S. Sewa, Polymer electrolyte actuator with gold electrodes, in: Y. Bar-Cohen (Ed), 1 ed., SPIE, Newport Beach, CA, USA, 1999, pp. 64–71.
 - [35] I. Takeuchi, K. Asaka, K. Kiyohara, T. Sugino, N. Terasawa, K. Mukai, T. Fukushima, T. Aida, Electromechanical behavior of fully plastic actuators based

- on bucky gel containing various internal ionic liquids, *Electrochimica Acta* 54 (2009) 1762–8.
- [36] F.D. Francesco, N. Calisi, M. Creatini, B. Melai, P. Salvo, C. Chiappe, Water sorption by anhydrous ionic liquids, *Green Chemistry* 13 (2011) 1712–7.
 - [37] A. Punning, A. Kruusmaa, A. Aabloo, Surface resistance experiments with IPMC sensors and actuators, *Sensors and Actuators a-Physical* 133 (2007) 200–9.
 - [38] S.M. Kim, K.J. Kim, Palladium buffer-layered high performance ionic polymer-metal composites, *Smart Materials & Structures* 17 (2008).
 - [39] U. Johanson, U. Mäeorg, V. Sammelselg, D. Brandell, A. Punning, M. Kruusmaa, A. Aabloo, Electrode reactions in Cu-Pt coated ionic polymer actuators, *Sensors and Actuators B: Chemical* 131 (2008) 340–6.
 - [40] M. Siripong, S. Fredholm, Q.A. Nguyen, B. Shih, J. Itescu, J. Stolk, A cost-effective fabrication method for ionic polymer-metal composites, in: V. Bharti, Y. BarCohen, Z.Y. Cheng, Q. Zhang, J. Madden (Eds), *Electroresponsive Polymers and Their Applications*, Materials Research Society, Warrendale, 2006, pp. 139–44.
 - [41] C.K. Chung, P.K. Fung, Y.Z. Hong, M.S. Ju, C.C.K. Lin, T.C. Wu, A novel fabrication of ionic polymer-metal composites (IPMC) actuator with silver nanopowders, *Sensors and Actuators B: Chemical* 117 (2006) 367–75.
 - [42] B.J. Akle, M.D. Bennett, D.J. Leo, High-strain ionomeric-ionic liquid electro-active actuators, *Sensors and Actuators a-Physical* 126 (2006) 173–81.
 - [43] B. Akle, S. Nawshin, D. Leo, Reliability of high strain ionomeric polymer transducers fabricated using the direct assembly process, *Smart Materials & Structures* 16 (2007) S256–S61.
 - [44] D.Y. Lee, I.-S. Park, M.-H. Lee, K.J. Kim, S. Heo, Ionic polymer-metal composite bending actuator loaded with multi-walled carbon nanotubes, *Sensors and Actuators A: Physical* 133 (2007) 117–27.
 - [45] K. Mukai, K. Asaka, T. Sugino, K. Kiyohara, I. Takeuchi, N. Terasawa, D. Futaba, K. Hata, T. Fukushima, T. Aida, Highly Conductive Sheets from Millimeter-Long Single-Walled Carbon Nanotubes and Ionic Liquids: Application to Fast-Moving, Low-Voltage Electromechanical Actuators Operable in Air, *Advanced Materials* 20 (2009) 1–4.
 - [46] T. Sugino, K. Kiyohara, I. Takeuchi, K. Mukai, K. Asaka, Improving the actuating response of carbon nanotube/ionic liquid composites by the addition of conductive nanoparticles, *Carbon* 49 (2011) 3560–70.
 - [47] J. Leis, M. Arulepp, A. Kuura, M. Lätt, E. Lust, Electrical double-layer characteristics of novel carbide-derived carbon materials, *Carbon* 44 (2006) 2122–9.
 - [48] A. Burke, Ultracapacitors: why, how, and where is the technology, *Journal of Power Sources* 91 (2000) 37–50.
 - [49] Y. Gogotsi, A. Nikitin, H. Ye, W. Zhou, J.E. Fischer, B. Yi, H.C. Foley, M.W. Barsoum, Nanoporous carbide-derived carbon with tunable pore size, *Nat Mater* 2 (2003) 591–4.
 - [50] R. Dash, J. Chmiola, G. Yushin, Y. Gogotsi, G. Laudisio, J. Singer, J. Fischer, S. Kucheyev, Titanium carbide derived nanoporous carbon for energy-related applications, *Carbon* 44 (2006) 2489–97.
 - [51] Y.J. Lee, J.C. Jung, S. Park, J.G. Seo, S.H. Baeck, J.R. Yoon, J. Yi, I.K. Song, Preparation and characterization of metal-doped carbon aerogel for supercapacitor, *Current Applied Physics* 10 (2010) 947–51.

- [52] J. Marie, R. Chenitz, M. Chatenet, S. Berthon-Fabry, N. Cornet, P. Achard, Highly porous PEM fuel cell cathodes based on low density carbon aerogels as Pt-support: Experimental study of the mass-transport losses, *Journal of Power Sources* 190 (2009) 423–34.
- [53] W. Lu, R. Hartman, L. Qu, L. Dai, Nanocomposite Electrodes for High-Performance Supercapacitors, *The Journal of Physical Chemistry Letters* 2 (2011) 655–60.
- [54] J. Torop, V. Palmre, M. Arulepp, T. Sugino, K. Asaka, A. Aabloo, Flexible supercapacitor-like actuator with carbide-derived carbon electrodes, *Carbon* 49 (2011) 3113–9.
- [55] B.S. Mitchell, *An introduction to materials engineering and science for chemical and materials engineers*, John Wiley, Hoboken, NJ, 2004.
- [56] A. Punning, U. Johanson, M. Anton, A. Aabloo, M. Kruusmaa, A Distributed Model of Ionomeric Polymer Metal Composite, *Journal of Intelligent Material Systems and Structures* 20 (2009) 1711–24.
- [57] H. Kurig, A. Janes, E. Lust, Electrochemical Characteristics of Carbide-Derived Carbon|1-Ethyl-3-methylimidazolium Tetrafluoroborate Supercapacitor Cells, *Journal of The Electrochemical Society* 157 (2010) A272-A9.
- [58] A. Jänes, L. Permann, P. Nigu, E. Lust, Influence of solvent nature on the electrochemical characteristics of nanoporous carbon|1 M (C₂H₅)₃CH₃NBF₄ electrolyte solution interface, *Surface Science* 560 (2004) 145–57.
- [59] P.I. Ravikovitch, A. Vishnyakov, A.V. Neimark, Density functional theories and molecular simulations of adsorption and phase transitions in nanopores, *Physical Review E* 64 (2001) 011602.
- [60] J. Leis, A. Perkson, M. Arulepp, P. Nigu, G. Svensson, Catalytic effects of metals of the iron subgroup on the chlorination of titanium carbide to form nanostructural carbon, *Carbon* 40 (2002) 1559–64.
- [61] E. Frackowiak, F. Béguin, Carbon materials for the electrochemical storage of energy in capacitors, *Carbon* 39 (2001) 937–50.
- [62] W. Sugimoto, T. Kizaki, K. Yokoshima, Y. Murakami, Y. Takasu, Evaluation of the pseudocapacitance in RuO₂ with a RuO₂/GC thin film electrode, *Electrochimica Acta* 49 (2004) 313–20.

7. SUMMARY IN ESTONIAN

Mikropoorsel süsinikul põhinevate elektroaktiivsete polümeersete aktuaatorite valmistamine ja karakteriseerimine

Käesolevas töös uuriti nelja erinevat poorset süsinikmaterjali (karbiidne süsinik, kookospähklikoores valmistatud aktiveeritud süsinik ning aktiveeritud ja mitteaktiveeritud süsinikaerogeelid) uute alternatiividena elektroaktiivsete polümeersete (EAP) aktuaatorite elektrootides. Vastavaid elektrootidmaterjale analüüsiti viiekihilistes aktuaator-süsteemides, mis koosenesid 1-etüül-3-metüülimidasoolium trifluorometaansulfonaat (EMI-TF) ioonvedelikus immutatud Nafion-membraanist kahe süsinikelektroodi vahel ja kuldfooliumist selle välispindadel. Uuriti valmistatud EAP aktuaatorite elektromehaanilisi, elektrokeemilisi ja mehaanilisi karakteristikuid ning võrreldi neid aktuaatoritega, mis baseerusid nii vettsisaldaval kui veevabal RuO₂-elektrootidel.

Karbiidsest süsinikust elektrootidega EAP aktuaator omas suurimat liigutusulatust (paine deformatsiooni) uuritud elektrootidmaterjalide seas. Vastav maksimaalne painde deformatsioon oli 2,04% ±2 V riskülikpinge sisendi korral, ületades RuO₂-elektrootidel põhineva aktuaatori liigutusulatust rohkem kui kaks korda. Karbiidsest süsinikust elektrootid omasid ka märkimisväärselt suuremat maksimaalset liigutuskiirust (kuni 0,23% sekundis), mis on ligi 2,5 korda kiirem liigutusest RuO₂-elektrootide korral. Seevastu aktiveeritud süsinik-elektrootidel põhinev aktuaator käitus suhteliselt sarnaselt RuO₂ elektrootidega. Maksimaalne painde deformatsioon mitteaktiveeritud ja aktiveeritud süsinikaerogeel- elektrootide korral oli vastavalt 1,3% ja 1,2%. Vastavad liigutuskiiirused olid kuni 0,15% sekundis ja 0,13% sekundis.

Tulemuste analüüs näitas, et EAP aktuaatorite elektromehaanilised karakteristikud on tugevalt sõltuvad süsinikmaterjalide poorsetest omadustest ja nende struktuurset jäikusest (st. grafitiseerituse astmest).

Karbiidsest süsinikust elektrootide oluliselt parem liigutussuutlikkus on peamiselt tingitud nende kõrgest krafitiseeritusest (5%) ja suurest eripinnast mikropoorses alas (0,7–0,8 nm), mis ühtib elektrolüüdi (EMI-TF) ioonide mõõtmatega. Mõlemad mainitud tegurid soodustavad suurema ruumalaefekti teket liigutusprotsessi käigus. Madalatemperatuursed N₂-sorptsiooni mõõtmised näitasid, et aktiveeritud ja mitteaktiveeritud süsinikaerogeelid omavad peaaegu identset poorset struktuuri mikropoorses alas, mis tingib ka nende sarnased liigutusomadused. Kuigi aktiveeritud süsinikaerogeel omab kõrgemat eripinda väiksemas mikropoorses alas (0,5–0,6 nm), on antud poorid liiga väikesed elektrolüüdi ioonide kiireks sisenemiseks. Röntgendifraktsioonanalüüsi tulemused näitasid, et süsinikaerogeelid (nii aktiveeritud kui mitteaktiveeritud) omavad täiesti amorfset struktuuri (grafitiseerituse aste 0%) ning on seetõttu oluliselt pehmemad ja elastsemad võrreldes karbiidse süsinikuga, mis omab mõõdetavat grafitiseerituse taset ning sisaldab mikroskoopseid grafiitseid

alasad. Seetõttu süsinikaerogeel-elektroodides liigutuse vältel elektrostaatilistest interaktsioonidest tingitud sisepinged hajutatakse süsinikmaatriksi kokkusurumises, mis omakorda tingib väiksema painde deformatsiooni tekke võrreldes karbiidset süsinikelektroodidel põhineva EAP aktuaatoriga.

Üheseinaliste süsiniknanotoru lisandite mõju aktuaatori liigutusomadustele uuriti kolmekihilistes aktuaator-süsteemides, mis koosensid polüvinülideenfluoriid-ko-heksafluoropropüleeni (PVdF(HFP)) ja 1-etüül-3-metüülimidasoolium tertrafluoroboraadi (EMI-BF₄) elektrolüüdikihist kahe nanotorusid ja karbiidset süsinikku sisaldava elektroodi kihi vahel. EAP aktuaatorid valmistati elektroodidega, mis sisaldasid süsiniknanotorusid karbiidset süsinik-elektroodis viies erinevas vahekorras ning uuriti nende elektromehaanilisi, elektrokeemilisi ja mehaanilisi omadusi. Tulemuste analüüs näitas, et suurendades süsiniknanotorude sisaldust komposiitelektroodides, parandas oluliselt elektroodide elektrilist juhtivust ning suurendas nende mehaanilist jäikust (Young'i moodulit). Süsiniknanotorude lisamine elektroodidesse suurendas märkimisväärselt aktuaatori liigutusulatust. Liigutusvõime paranemine kõrgematel liigutussagedustel (0,5–50 Hz) on peamiselt tingitud paremast elektroodi juhtivusest ja kõrgemast mesoporsuset, mis tagab kiirema elektrolüüdi ioonide juurdepääsu poorsesse elektroodimaatriksisse. Madalamatel liigutussagedustel (5 mHz–0,5 Hz) oli aktuaatoril, mille elektroodid sisaldasid võrdses koguses nanotorusid ja karbiidset süsinikku (50/50 massi%), oluliselt suurem liigutusulatus (deformatsioon 0,85%) uuritud aktuaatorite seas. See ületab puhtast karbiidset süsinikust elektroodidega aktuaatori liigutusulatust (0,35%) rohkem kui kaks korda. Süsiniknanotorud ja karbiidne süsinik suhtes 50/50 omas samuti parimat kombinatsiooni paindejõus ja maksimaalses liigutusulatuses. Leiti, et erimahtuvus ja Youngi moodul omavad tugevat koosmõju aktuaatori liigutusulatusele madalamas sagedusalas. Tuletatud korrelatsioon mainitud parameetrite vahel näitas, et nanotorud/karbiidne süsinik 50/50 suhte oluliselt suurem liigutusvõime on tingitud mikro- ja mesoporsuse ainulaadsest tasakaalust EAP elektroodides ja mõõdukalt kõrge süsinikmaatriksi jäikusest.

8. ACKNOWLEDGEMENTS

First and foremost I would like to thank my supervisors Prof. Enn Lust and Prof. Alvo Aabloo for their guidance and support throughout my doctoral studies.

Also, I would like to thank all of my collaborators, colleagues and friends, especially Prof. Kwang Kim, Janno Torop and David Pugal.

I would like to thank the Archimedes Foundation and Estonian Science Foundation for financial support.

Last but not least, I would like to express my deepest gratitude to my family, especially to my wife Kaili and my son Robert for their support, patience and encouragement during my studies.

9. ORIGINAL PUBLICATIONS

CURRICULUM VITAE

Viljar Palmre

Date of birth: January 9th, 1984
Citizenship: Estonian
Marital status: married, one child
Address: IMS Lab, Institute of Technology
University of Tartu
Nooruse 1, 50411 Tartu, Estonia
Phone: +372 737 5534
E-mail: viljarp@ut.ee

Education

2008–... University of Tartu, *Ph.D.* student (Materials Science)
2006–2008 University of Tartu, *M.Sc.* in Materials Science, 2008
2003–2006 University of Tartu, *B.Sc.* in Materials Science, 2006

Publications

- [1] V. Palmre, J. Torop, M. Arulepp, T. Sugino, K. Asaka, A. Jänes, E. Lust, A. Aabloo, Impact of carbon nanotube additives on carbide-derived carbon-based electroactive polymer actuators. *Carbon* (2012). Accepted.
- [2] V. Palmre, E. Lust, A. Jänes, M. Koel, A.-L. Peikolainen, J. Torop, U. Johanson, A. Aabloo, Electroactive polymer actuators with carbon aerogel electrodes, *Journal of Materials Chemistry* 21 (2011) 2577–83.
- [3] V. Palmre, D. Brandell, U. Mäeorg, J. Torop, O. Volobujeva, A. Punning, U. Johanson, M. Kruusmaa, A. Aabloo, Nanoporous carbon-based electrodes for high strain ionomeric bending actuators, *Smart Materials & Structures* 18 (2009).
- [4] J. Torop, M. Arulepp, J. Leis, A. Punning, U. Johanson, V. Palmre, A. Aabloo, Nanoporous carbide-derived carbon material-based linear actuators. *Materials* 3 (1) (2010) 9–25.
- [5] J. Torop, V. Palmre, M. Arulepp, T. Sugino, K. Asaka, A. Aabloo, Flexible supercapacitor-like actuator with carbide-derived carbon electrodes, *Carbon* 49 (2011) 3113–9.
- [6] V. Palmre, D. Brandell, U. Maeorg, J. Torop, O. Volobujeva, A. Punning, U. Johanson, A. Aabloo, Ionic polymer metal composites with nanoporous carbon electrodes, in: Y. Bar-Cohen (Ed), 1 ed., SPIE, San Diego, CA, USA, 2010, pp. 76421D-9.

- [7] J.J. Hubbard, M. Fleming, K.K. Leang, V. Palmre, D. Pugal, K.J. Kim, Characterization of Sectored-Electrode IPMC-Based Propulsors for Underwater Locomotion, ASME Conference Proceedings 2011 (2011) 171–80.
- [8] V. Palmre, S.J. Kim, K. Kim, Millimeter thick ionic polymer membrane-based IPMCs with bimetallic Pd-Pt electrodes, in: Y. Bar-Cohen, F. Carpi (Eds), 1 ed., SPIE, San Diego, California, USA, 2011, pp. 797615 (2011).
- [9] V. Palmre, D. Pugal, K. Kim, Characterization of longitudinal tensile force of millimeter thick IPMCs, in: Y. Bar-Cohen (Ed), 1 ed., SPIE, San Diego, California, USA, 2012, pp. 83402L-8.
- [10] D. Pugal, K.J. Kim, V. Palmre, K.K. Leang, A. Aabloo, Physics-based electromechanical model of IPMC considering various underlying currents, in: Y. Bar-Cohen (Ed), 1 ed., SPIE, San Diego, California, USA, 2012, pp. 83400P-10.
- [11] D. Kim, K.J. Kim, J.-d. Nam, V. Palmre, Electro-chemical operation of ionic polymer-metal composites, Sensors and Actuators B-Chemical 155 (2011) 106–13.

ELULOOKIRJELDUS

Viljar Palmre

Sünniaeg: 9. jaanuar 1984
Kodakondsus: Eesti
Perekonnaseis: abielus, üks laps
Aadress: IMS Lab, Tehnoloogiainstituut
Tartu Ülikool
Nooruse 1, 50411 Tartu, Eesti
Telefon: +372 737 5534
E-mail: viljarp@ut.ee

Haridus

2008–... Tartu Ülikool, doktorant (materjaliteadus)
2006–2008 Tartu Ülikool, *M.Sc.* materjaliteaduse erialal, 2008
2003–2006 Tartu Ülikool, *B.Sc.* materjaliteaduse erialal, 2006

Publikatsioonid

- [1] V. Palmre, J. Torop, M. Arulepp, T. Sugino, K. Asaka, A. Jänes, E. Lust, A. Aabloo, Impact of carbon nanotube additives on carbide-derived carbon-based electroactive polymer actuators. *Carbon* (2012). Accepted.
- [2] V. Palmre, E. Lust, A. Jänes, M. Koel, A.-L. Peikolainen, J. Torop, U. Johanson, A. Aabloo, Electroactive polymer actuators with carbon aerogel electrodes, *Journal of Materials Chemistry* 21 (2011) 2577–83.
- [3] V. Palmre, D. Brandell, U. Mäeorg, J. Torop, O. Volobujeva, A. Punning, U. Johanson, M. Kruusmaa, A. Aabloo, Nanoporous carbon-based electrodes for high strain ionomeric bending actuators, *Smart Materials & Structures* 18 (2009).
- [4] J. Torop, M. Arulepp, J. Leis, A. Punning, U. Johanson, V. Palmre, A. Aabloo, Nanoporous carbide-derived carbon material-based linear actuators. *Materials* 3 (1) (2010) 9–25.
- [5] J. Torop, V. Palmre, M. Arulepp, T. Sugino, K. Asaka, A. Aabloo, Flexible supercapacitor-like actuator with carbide-derived carbon electrodes, *Carbon* 49 (2011) 3113–9.
- [6] V. Palmre, D. Brandell, U. Maeorg, J. Torop, O. Volobujeva, A. Punning, U. Johanson, A. Aabloo, Ionic polymer metal composites with nanoporous carbon electrodes, in: Y. Bar-Cohen (Ed), 1 ed., SPIE, San Diego, CA, USA, 2010, pp. 76421D-9.
- [7] J.J. Hubbard, M. Fleming, K.K. Leang, V. Palmre, D. Pugal, K.J. Kim, Characterization of Sectored-Electrode IPMC-Based Propulsors for Underwater Locomotion, *ASME Conference Proceedings* 2011 (2011) 171–80.

- [8] V. Palmre, S.J. Kim, K. Kim, Millimeter thick ionic polymer membrane-based IPMCs with bimetallic Pd-Pt electrodes, in: Y. Bar-Cohen, F. Carpi (Eds), 1 ed., SPIE, San Diego, California, USA, 2011, pp. 797615 (2011).
- [9] V. Palmre, D. Pugal, K. Kim, Characterization of longitudinal tensile force of millimeter thick IPMCs, in: Y. Bar-Cohen (Ed), 1 ed., SPIE, San Diego, California, USA, 2012, pp. 83402L-8.
- [10] D. Pugal, K.J. Kim, V. Palmre, K.K. Leang, A. Aabloo, Physics-based electromechanical model of IPMC considering various underlying currents, in: Y. Bar-Cohen (Ed), 1 ed., SPIE, San Diego, California, USA, 2012, pp. 83400P-10.
- [11] D. Kim, K.J. Kim, J.-d. Nam, V. Palmre, Electro-chemical operation of ionic polymer-metal composites, *Sensors and Actuators B-Chemical* 155 (2011) 106–13.

DISSERTATIONES SCIENTIAE MATERIALIS

UNIVERSITATIS TARTUENSIS

1. **Martin Järvekülg.** Tubular microstructures by Hf-, Zr- and Ti-butoxide gel sheet rolling. Tartu, 2011, 112 p.
2. **Sergei Vlassov.** Investigation of nanoscale interactions and mechanical properties of nanostructures using quartz tuning fork based real-time measurements. Tartu, 2011, 171 p.
3. **Margus Kodu.** Pulsed Laser Deposition of Magnesium Oxide and Barium Ternary Oxides for Plasma Display Protective Layers. Tartu, 2011, 89 p.
4. **Rainer Pärna.** Surface studies of some oxide films. Tartu, 2011, 129 p.
5. **Jevgeni Šulga.** Self-assembly and interaction of nanostructures. Tartu, 2011, 114 p.
6. **Wojciech Kuznik.** Quantum-chemical computer simulations of the linear and non-linear optical properties of pyrazoloquinoline and dicyanopyrazine derivatives. Tartu, 2012, 89 p.
7. **Leonid Dorogin.** Structural and tribological properties of zero- and one-dimensional nanocrystals. Tartu, 2012, 193 p.